NASA CONTRACTOR REPORT

NASA CR-2777

NASA CR-2

A GENERAL METHOD FOR CALCULATING THREE-DIMENSIONAL COMPRESSIBLE LAMINAR AND TURBULENT BOUNDARY LAYERS ON ARBITRARY WINGS

Tuncer Cebeci, Kalle Kaups, and Judy A. Ramsey

Prepared by
MCDONNELL DOUGLAS CORPORATION
Long Beach, Calif. 90846
for Langley Research Center

NATIONAL AERONAUTICS AND SPACE ADMINISTRATION • WASHINGTON, D. C. • JANUARY 1977

0061384

1. Report No. NASA CR-2777	2. Government Accession No.	3. Recipient's Catalog No.
4. Title and Subtitle A General Method for Calculating Three-Dimensional Compressible Laminar and Turbulent Boundary Layers on Arbitrary Wings		5. Report Date January 1977
		6. Performing Organization Code
7. Author(s) Tuncer Cebeci, Kalle Kaups, and Judy A. Ramsey		8. Performing Organization Report No.
		10. Work Unit No.
9. Performing Organization Name and Address McDonnell Douglas Corporation 3855 Lakewood Blvd, Long Beach, California 90846		11. Contract or Grant No. NAS1-12821
		13. Type of Report and Period Covered Contractor Report November 1973 - March 1976
12. Sponsoring Agency Name and Address National Aeronautics and Space Administration Washington, DC 20546		14. Sponsoring Agency Code

15. Supplementary Notes

Langley technical monitor: Stephen F. Wornom

Topical report.

16. Abstract

A very general method for calculating three-dimensional compressible laminar and turbulent boundary layers on arbitrary wings is described. The method utilizes a nonorthogonal coordinate system for the boundary-layer calculations and includes a geometry program that represents the wing analytically, and a velocity program that computes the external velocity components from a given experimental pressure distribution when the external velocity distribution is not computed theoretically. The boundary-layer method is general, however, and can also be used for an external velocity distribution computed theoretically.

Several test cases are computed by this method and the results are checked with other numerical calculations and with experiment when available. A typical computation time (CPU) on an IBM 370/165 computer for one surface of a wing which roughly consist of 30 spanwise stations and 25 streamwise stations, with 30 points across the boundary layer is less than 30 seconds for an incompressible flow and is a little over this for a compressible flow.

17. Key Words (Suggested by Author(s)) Boundary layers	18. Distribution Statement Unclassified - Unlimited Subject Category 02

19. Security Classif. (of this report) Unclassified	20. Security Classif. (of this page) Unclassified	21. No. of Pages 87	22. Price* $4.75

* For sale by the National Technical Information Service, Springfield, Virginia 22161

A GENERAL METHOD FOR CALCULATING THREE-DIMENSIONAL COMPRESSIBLE LAMINAR AND TURBULENT BOUNDARY LAYERS ON ARBITRARY WINGS

by

Tuncer Cebeci, Kalle Kaups, and Judy A. Ramsey
McDonnell Douglas Corporation

SUMMARY

A very general method for calculating three-dimensional compressible laminar and turbulent boundary layers on arbitrary wings is described. The method utilizes a nonorthogonal coordinate system for the boundary-layer calculations and includes a geometry program that represents the wing analytically, and a velocity program that computes the external velocity components from a given experimental pressure distribution when the external velocity distribution is not computed theoretically. The boundary-layer method is general, however, and can also be used for an external velocity distribution computed theoretically.

The boundary-layer method accounts for all the geometric parameters of the coordinate system. The Reynolds shear-stress terms are modeled by an eddy-viscosity formulation developed by Cebeci. The governing equations are solved by a two-point finite-difference method used earlier by Keller and Cebeci for two-dimensional flows and later by Cebeci for three-dimensional flows.

Several test cases are computed by this method and the results are checked with other numerical calculations and with experiment when available. A typical computation time (CPU) on an IBM 370/165 computer for one surface of a wing which roughly consist of 30 spanwise stations and 25 streamwise stations, with 30 points across the boundary layer is less than 30 seconds for an incompressible flow and is a little over this for a compressible flow.

TABLE OF CONTENTS

A	Van Driest damping length
b	$C(1 + \varepsilon_m^+)$ or a constant for scaling the spanwise coordinate y
c	ρ_e/ρ or local chord length
cf_c	local skin-friction coefficient based on the Cartesian component of wall shear stress vector in x-coordinate direction
cf_n	local skin-friction coefficient based on the Cartesian component of wall shear stress vector normal to the x-y-plane.
C	$\rho\mu/(\rho_e\mu_e)$
C_p	pressure coefficient, $2(p - p_\infty)/(\rho_\infty u_\infty^2)$
E	total enthalpy ratio, H/H_e
f	transformed vector potential for ψ
f'	u/u_e
g	transformed vector potential for ϕ
g'	w/u_{ref}
G	E'
H	total enthalpy
i,j,k	unit vectors in $\bar{x},\bar{y},\bar{z}$-directions of the Cartesian coordinate system in which the wing is defined.
$K_1 = K_{g_1}$, $K_2 = K_{g_2}$	geodesic curvatures
K_{12}, K_{21}	geometric parameters
$\vec{K}$	curvature vector of (3-D) coordinate line
L	modified mixing-length or a scaling constant
$m_1, m_2, m_3, \ldots$	parameters in transformed differential equations
M_∞	free-stream Mach number
$\vec{n}$	unit outside normal vector to the surface
p	static pressure

Pr	Prandtl number
P_T	total pressure
$\vec{r}$	$(\bar{x}, \bar{y}, \bar{z})$ position vector for point on surface
Re	$u_e s_1 / \nu_e$, Reynolds number
s_1	arc length along x-coordinate line
t	time
$\vec{t}$	unit tangent vector along (3-D) coordinate line
u	component of velocity vector in x-coordinate direction
u_{ref}	reference velocity
u_s	resultant velocity at the edge of boundary layer
u_t	total or resultant velocity
u_x	derivative $\partial u / \partial x$
u_τ	friction velocity
u_∞	free-stream velocity
v	component of velocity vector normal to the surface
w	component of velocity vector in z-coordinate direction
w_z	$\partial w / \partial z$
$-\rho \overline{u'v'}, -\rho \overline{w'v'}, -\rho \overline{v'H'}$	Reynolds stresses
x	independent variable in chordwise direction, $x = \phi - \phi_0$ (attachment line)
y	independent variable normal to the surface, is equal to the normal distance.
z	independent variable in spanwise direction, $z = \bar{y}/b$
$\bar{x}, \bar{y}, \bar{z}$	Cartesian coordinate system used for wing definition
α	local geometric angle of attack of wing section chord lines with respect to $\bar{x}$-axis ($\alpha(\bar{y})$ expresses wing twist)
α	constant in outer eddy viscosity equal to 0.0168

β	flow deflection angle
γ	isentropic exponent, here $\gamma = 1.4$
δ_c^*	displacement thickness based on the Cartesian velocity components in the x-coordinate direction
δ_n^*	displacement thickness based on the Cartesian velocity components normal to the xy-plane
ε (or ε_m), ε_H	eddy viscosity and eddy conductivity, respectively
ζ	airfoil ordinate in the coordinate system defined in figure B2.
η	transformed coordinate normal to surface
θ	angle in tangent plane between x and z coordinate lines
θ_c	momentum thickness based on the Cartesian velocity components in the x-coordinate direction
θ_n	momentum thickness based on the Cartesian velocity components normal to the xy-plane
λ	local sweep angle, measured between normal plane to freestream velocity vector and z-coordinate line
μ	dynamic viscosity
μ_1, μ_2, μ_3	parameters in transformed energy equation
ν	kinematic viscosity
ξ	airfoil abscissa in the coordinate system defined in figure A2
ρ	density
τ	shear stress
ϕ	stretching variable defined by eq. (B5) (x-coordinate in differential equation is $x = \phi - \phi_0$ (attachment line))
Φ, ψ	two-component vector potential, eq. (33)

Subscripts

e	outer edge, effective
g	geodesic
i	at chordwise input stations

i,o	inner and outer regions for eddy viscosity
j	at spanwise input stations
ℓ	leading edge
p	chordwise stations at which boundary layer is computed
r	wing root
s	spanwise stations at which boundary layer is computed
t	wing tip or "total"
w	wall
∞	free-stream conditions

bars denote Cartesian coordinate system

primes denote differentiation with respect to η

INTRODUCTION

In recent years several methods have been developed to compute three-dimensional laminar and turbulent boundary layers. For example, in [1], Hunt, Bushnell and Beckwith developed a finite-difference method for analyzing compressible turbulent boundary layers on a blunt swept slab with leading edge blowing. In that reference, the Reynolds shear stress terms were modeled by using a mixing-length expression which was based on a generalization of the two-dimensional model used earlier by Bushnell and Beckwith [2]. This model has been adapted by Adams and was used to compute several semi-three-dimensional turbulent boundary layers (see, for example, [3]). In [4] Bradshaw extended his two-dimensional method to compute three-dimensional flows past infinite swept wings and obtained good agreement with experiment. His method differs from the previously mentioned ones in that his modeling of the Reynolds shear-stress terms does not use the mixing-length concepts; rather, it uses the turbulence kinetic energy equation, a model that has been used extensively by Nash and his associates (see, for example, [5], [6]). Recently Harris and Morris [7], Kendall et al. [8], and Wortman [9], developed methods to compute full three-dimensional compressible laminar and turbulent boundary layers. Their methods also use mixing-length, eddy-viscosity concepts to model the Reynolds stresses. Except for the methods of Kendall et al. and Wortman, none of the above-mentioned methods have been applied to flow problems over real aerodynamic configurations such as wings, and the problems of calculating three-dimensional laminar and turbulent boundary layers on such bodies have never been investigated.

In the present report, we discuss a general method applicable to three-dimensional compressible laminar and turbulent boundary-layer flows on arbitrary wings. The method uses an eddy-viscosity formulation developed by Cebeci [10] and uses a two-point finite-difference method developed by Keller and Cebeci [11]. So far this method has been tested for most of the available experimental data on various three-dimensional flows and has been found to give accurate results (see, for example, [10], [12], [13]).

The three-dimensional method presented here has a number of desirable features. First, it uses a very convenient coordinate system to do the boundary-layer calculations. This is a nonorthogonal system that eliminates most of the computational difficulties associated with the orthogonal systems used for wing problems. To illustrate this significant feature, let us consider an orthogonal system in which the orthogonals are constructed at constant percent-chord stations. With this system, as shown in figure 1, the orthogonals started from the wing-root congregate at the nose, leaving large portions near the trailing edge uncovered. This is especially true for a wing with a sharp trailing edge. A round trailing edge rectifies the situation somewhat but there is still a large area of the wing where the orthogonals are sparce.

The coordinate system in figure 1 was constructed with the polar angle $\phi = x$ at the root section as the other surface coordinate (see figure B2). As is seen from figure 1, there are computational difficulties at the trailing edge. To show this, consider figure 2 in which the surface coordinate network x and z is obtained by extending the surface coverage with the
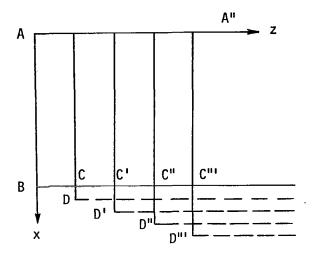
Figure 1. An orthogonal system for the wing.

Figure 2. Wing in the x and z plane.

dashed lines. Here AA" is the stagnation line, AB the root section, and D is a point on the trailing edge. Starting from the initial lines, the boundary layer can be calculated along the line BC" including the root. However, the point D cannot be obtained in a straightforward manner. This is also true for the rest of the trailing edge points D', D" and D'".

Another possible coordinate system can be obtained by representing the wing by one or more separate conical surfaces. Figure 3 shows such a representation. Here the wing panels ABDC and CDFE form two conical surfaces with apexes at P and Q, respectively. The shape of the panel ABDC and the coordinate system in the developed plane are shown in figure 4. The initial lines are AC and AB. AC is the stagnation line and AB is the wing fuselage junction. Calculations can be started at corner A. A linear coordinate transformation can be used to avoid marching into the negative r direction. Such a coordinate system without taking the thickness into account (this amounts to representing wing sections by flat plates) was
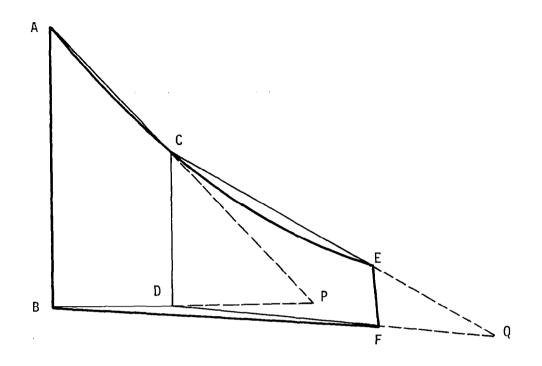
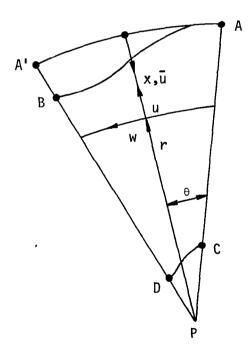Figure 3. Representation of the wing by conical sections.

Figure 4. Notation for conical section ABDC and the coordinate system in the developed plane.

4

used by Nash and Scruggs [6].   The disadvantage of this coordinate system
is the difficulty of doing calculations in the overlap region.   This is a
major difficulty and with the assumption for zero thickness, it is a poor
and inaccurate coordinate system for boundary-layer computations.

A second major desirable feature of our method is the geometry subprogram
which is employed to calculate the coordinate system and its geometrical param-
eters.   By means of this program, since we are using a body-oriented coordinate
system, we represent the wing analytically and calculate the geodesic curva-
tures and the metric coefficients once and for all.   In this way we eliminate
the need for calculating the coordinate system, say, with each angle of attack,
as in the case with a streamline coordinate system,

A third desirable feature of our method is its extremely short computa-
tion time.   According to our calculations, we observe that a typical computa-
tion time (CPU) on an IBM 370/165 computer for one surface of a wing, which
roughly consists of 30 spanwise stations and 25 chordwise stations with 30
grid points across the layer, is less than 30 seconds for an incompressible
flow and slightly more for a compressible flow.   There are several reasons
for such a small computation time.   First, we use transformed variables that
allow us to take a few spanwise and chordwise stations.   Second, our coordi-
nate system is an "optimum" coordinate system for a wing, the flow on one
streamwise section differs little from the other neighboring streamwise
sections, making the numerical solutions converge very rapidly.   A third,
and maybe the most important reason, is the numerical method we use.   This
is a very efficient scheme that has been found to be very suitable for
parabolic partial differential equations (see, for example, [14]).

The method so far has been demonstrated for several test cases and its
accuracy has been checked with experimental data and with other numerical cal-
culations.   The results look very encouraging.   However, additional calcula-
tions are needed to further test the method for flow conditions other than
those studied here.

GOVERNING EQUATIONS

The governing boundary-layer equations for a nonorthogonal coordinate system are given in references [15] and [16]. With a slight change of notation for compressible laminar and turbulent flows (x and z denoting the surface coordinates (see figure 5)), they are given by

Continuity equation

$$\frac{\partial}{\partial x}(\rho u h_2 \sin\theta) + \frac{\partial}{\partial z}(\rho w h_1 \sin\theta) + \frac{\partial}{\partial y}(\overline{\rho v}h_1 h_2 \sin\theta) = 0 \tag{1}$$
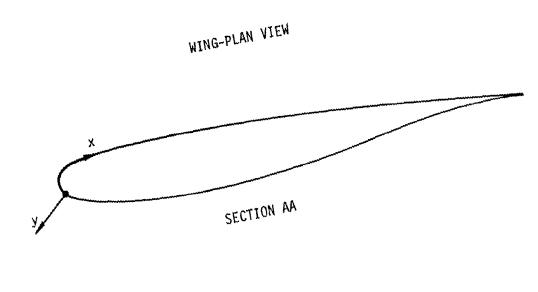
x-Momentum equation

$$\rho \frac{u}{h_1}\frac{\partial u}{\partial x} + \rho \frac{w}{h_2}\frac{\partial u}{\partial z} + \overline{\rho v}\frac{\partial u}{\partial y} - \rho \cot\theta \, K_1 u^2 + \rho\csc\theta \, K_2 w^2 + \rho K_{12} uw$$

$$= -\frac{\csc^2\theta}{h_1}\frac{\partial p}{\partial x} + \frac{\cot\theta \, \csc\theta}{h_2}\frac{\partial p}{\partial z} + \frac{\partial}{\partial y}\left(\mu\frac{\partial u}{\partial y} - \rho\overline{u'v'}\right) \tag{2}$$

z-Momentum equation

$$\rho \frac{u}{h_1}\frac{\partial w}{\partial x} + \rho \frac{w}{h_2}\frac{\partial w}{\partial z} + \overline{\rho v}\frac{\partial w}{\partial y} - \rho \cot\theta \, K_2 w^2 + \rho\csc\theta \, K_1 u^2 + \rho K_{21} uw$$

$$= \frac{\cot\theta \, \csc\theta}{h_1}\frac{\partial p}{\partial x} - \frac{\csc^2\theta}{h_2}\frac{\partial p}{\partial z} + \frac{\partial}{\partial y}\left(\mu\frac{\partial w}{\partial y} - \rho\overline{w'v'}\right) \tag{3}$$

Energy equation

$$\rho \frac{u}{h_1}\frac{\partial H}{\partial x} + \rho \frac{w}{h_2}\frac{\partial H}{\partial z} + \overline{\rho v}\frac{\partial H}{\partial y} = \frac{\partial}{\partial y}\left[\frac{\mu}{Pr}\frac{\partial H}{\partial y} + \mu\left(1 - \frac{1}{Pr}\right)\frac{\partial}{\partial y}\left(\frac{u_t^2}{2}\right) - \rho\overline{v'H'}\right] \tag{4}$$
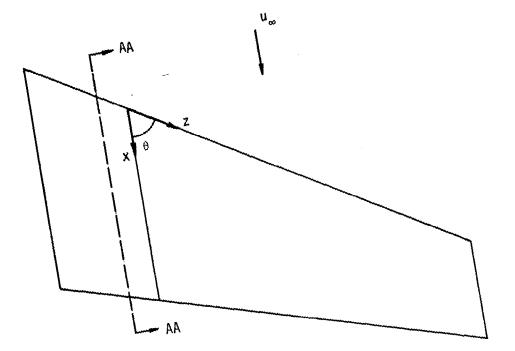
Here $\overline{\rho v} = \rho v + \overline{\rho'v'}$ and h_1 and h_2 are metric coefficients. The latter are functions of x and z, that is,

$$h_1 = h_1(x,z) \quad , \quad h_2 = h_2(x,z) \tag{5}$$

Also, θ represents the angle between the coordinate lines x and z. For an orthogonal system $\theta = \pi/2$. The parameters K_1 and K_2 are known as the geodesic curvatures of the curves z = const. and x = const., respectively. They are given by

u_∞

AA

θ

z

x

AA

WING-PLAN VIEW

x

y

SECTION AA

coordinate system for a swept wing.

$$K_1 = \frac{1}{h_1 h_2 \sin\theta} \left[\frac{\partial}{\partial x} (h_2 \cos\theta) - \frac{\partial h_1}{\partial z} \right], \quad K_2 = \frac{1}{h_1 h_2 \sin\theta} \left[\frac{\partial}{\partial z} (h_1 \cos\theta) - \frac{\partial h_2}{\partial x} \right] \tag{6}$$

The parameters K_{12} and K_{21} are defined by

$$K_{12} = \frac{1}{\sin\theta} \left[-\left(K_1 + \frac{1}{h_1} \frac{\partial\theta}{\partial x}\right) + \cos\theta \left(K_2 + \frac{1}{h_2} \frac{\partial\theta}{\partial z}\right) \right] \tag{7a}$$

$$K_{21} = \frac{1}{\sin\theta} \left[-\left(K_2 + \frac{1}{h_2} \frac{\partial\theta}{\partial z}\right) + \cos\theta \left(K_1 + \frac{1}{h_1} \frac{\partial\theta}{\partial x}\right) \right] \tag{7b}$$

u_t represents the total velocity within the boundary layer and is given by

$$u_t = (u^2 + w^2 + 2uw \cos\theta)^{1/2} \tag{8}$$

At the edge of the boundary layer, (2) and (3) reduce to

$$\rho_e \left(\frac{u_e}{h_1} \frac{\partial u_e}{\partial x} + \frac{w_e}{h_2} \frac{\partial u_e}{\partial z} - \cot\theta \, K_1 u_e^2 + \csc\theta \, K_2 w_e^2 + K_{12} u_e w_e \right)$$
$$= -\frac{\csc^2\theta}{h_1} \frac{\partial p}{\partial x} + \frac{\cot\theta \csc\theta}{h_2} \frac{\partial p}{\partial z} \tag{9}$$

$$\rho_e \left(\frac{u_e}{h_1} \frac{\partial w_e}{\partial x} + \frac{w_e}{h_2} \frac{\partial w_e}{\partial z} - \cot\theta \, K_2 w_e^2 + \csc\theta \, K_1 u_e^2 + K_{21} u_e w_e \right)$$
$$= \frac{\cot\theta \csc\theta}{h_1} \frac{\partial p}{\partial x} - \frac{\csc^2\theta}{h_2} \frac{\partial p}{\partial z} \tag{10}$$

The boundary conditions which we shall consider for (1) - (4) are:

$$y = 0 \qquad u, v, w = 0, \qquad \left(\frac{\partial H}{\partial y}\right)_w = 0 \tag{11a}$$

$$y = \delta \qquad u = u_e(x,z), \qquad w = w_e(x,z), \qquad H = H_e \tag{11b}$$

The solution of the system given by (1) - (4) subject to (11) requires closure assumptions for the Reynolds stresses, $-\rho\overline{u'v'}$, $-\rho\overline{w'v'}$ and $-\rho\overline{v'H'}$. They also require initial conditions on two intersecting planes. Here we consider several options of starting initial conditions on these planes. When the solutions start at the leading edge of the wing, we use the stagnation-line equations. These equations are obtained in the present coordinate

system be examining the velocity components in the coordinate system shown in figure 6 where we see that

$$\overline{u} = u\ \sin\theta$$

$$\overline{w} = w + u\cdot\cos\theta$$

At the stagnation line $\overline{u} = 0$. Therefore, $u = 0$ and $w = \overline{w}$. Thus, equations (1), (2), and (3) reduce to the stagnation-line equations if we set $u \equiv \partial p/\partial x = 0$. Then the x-momentum equation becomes singular on that line. However, differentiation with respect to x will yield a nonsingular equation. After performing the necessary differentiation for the x-momentum equation and taking advantage of approximate symmetry conditions $(\partial w/\partial x = \partial v/\partial x = \partial^2 u/\partial x^2 = 0)$ and using (9) and (10), we can write the governing <u>stagnation-line</u> equations as:

Figure 6. Sketch showing the coordinate velocity components in orthogonal and nonorthogonal systems.

Continuity:

$$\rho h_2\ \sin\theta\ u_x + \frac{\partial}{\partial z}\left(\rho w h_1\ \sin\theta\right) + \frac{\partial}{\partial y}\left(\overline{\rho v}h_1 h_2\ \sin\theta\right) = 0 \qquad (12)$$

x-Momentum:

$$\rho\frac{u_x^2}{h_1} + \rho\frac{w}{h_2}\frac{\partial u_x}{\partial z} + \overline{\rho v}\frac{\partial u_x}{\partial y} + \rho K_{12}w u_x = \rho_e\left(\frac{u_{xe}^2}{h_1} + \frac{w_e}{h_2}\frac{\partial u_{xe}}{\partial x} + K_{12}w_e u_{xe}\right)$$

$$+ \frac{\partial}{\partial y}\left[\mu\frac{\partial u_x}{\partial y} - \rho(\overline{u'v'})_x\right] \qquad (13)$$

9

z-Momentum:

$$\rho \frac{w}{h_2} \frac{\partial w}{\partial z} + \overline{\rho v} \frac{\partial w}{\partial y} - \rho \cot\theta \, K_2 w^2 = \rho_e \left(\frac{w_e}{h_2} \frac{\partial w_e}{\partial z} - \cot\theta \, K_2 w_e^2 \right)$$

$$+ \frac{\partial}{\partial y} \left(\mu \frac{\partial w}{\partial y} - \rho \overline{w'v'} \right) \tag{14}$$

Energy

$$\rho \frac{w}{h_2} \frac{\partial H}{\partial z} + \overline{\rho v} \frac{\partial H}{\partial y} = \frac{\partial}{\partial y} \left[\frac{\mu}{Pr} \frac{\partial H}{\partial y} + \mu \left(1 - \frac{1}{Pr} \right) \frac{\partial}{\partial y} \left(\frac{u_t^2}{2} \right) - \rho \overline{v'H'} \right] \tag{15}$$

Here $u_x = \partial u / \partial x$, $u_{xe} = \partial u_e / \partial x$ and total velocity $u_t = w$. These equations are subject to the following boundary conditions

$$y = 0, \qquad u_x, \, v, \, w = 0, \qquad (\partial H / \partial y)_w = 0 \tag{16a}$$

$$y = \delta \qquad u_x = u_{xe}(x,z), \qquad w = w_e(x,z), \qquad H = H_e \tag{16b}$$

When the solutions start at the root or the tip of the wing, excluding the leading edge, we use either the chordwise attachment-line equations (plane of symmetry) or the infinite-swept-wing equations. Note that these equations are just approximations to the governing equations in those two regions. The attachment-line equations are obtained in a manner similar to the stagnation-line equations. On this line w and $\partial p / \partial z$ are zero making the z-momentum equation singular. However, differentiation with respect to z yields a nonsingular equation. After performing the necessary differentiation for the z-momentum and taking advantage of the approximate symmetry conditions $(\partial u / \partial z = \partial v / \partial z = \partial^2 w / \partial z^2 = 0)$ and using (9) and (10), we can write the governing chordwise attachment-line equations as:

Continuity:

$$\frac{\partial}{\partial x} (\rho u h_2 \sin\theta) + \rho h_1 \sin\theta \, w_z + \frac{\partial}{\partial y} (\overline{\rho v} h_1 h_2 \sin\theta) = 0 \tag{17}$$

x-Momentum

$$\rho \frac{u}{h_1} \frac{\partial u}{\partial x} + \overline{\rho v} \frac{\partial u}{\partial y} - \rho \cot\theta \, K_1 u^2 = \rho_e \left(\frac{u_e}{h_1} \frac{\partial u_e}{\partial x} - \cot\theta \, K_1 u_e^2 \right)$$

$$+ \frac{\partial}{\partial y} \left(\mu \frac{\partial u}{\partial y} - \rho \overline{u'v'} \right) \tag{18}$$

10

z-Momentum

$$\rho \frac{u}{h_1} \frac{\partial w_z}{\partial x} + \frac{\rho}{h_2} w_z^2 + \overline{\rho v} \frac{\partial w_z}{\partial y} + \rho K_{21} u w_z = \rho_e \left(\frac{u_e}{h_1} \frac{\partial w_{ze}}{\partial x} + \frac{w_{ze}^2}{h_2} + K_{21} u_e w_{ze} \right)$$
$$+ \frac{\partial}{\partial y} \left[\mu \frac{\partial w_z}{\partial y} - \rho (\overline{w'v'})_z \right] \qquad (19)$$

Energy

$$\rho \frac{u}{h_1} \frac{\partial H}{\partial x} + \overline{\rho v} \frac{\partial H}{\partial y} = \frac{\partial}{\partial y} \left[\frac{\mu}{Pr} \frac{\partial H}{\partial y} + \mu \left(1 - \frac{1}{Pr} \right) \frac{\partial}{\partial y} \left(\frac{u_t^2}{2} \right) - \rho \overline{v'H'} \right] \qquad (20)$$

Here $w_z = \partial w / \partial z$, $w_{ze} = \partial w_e / \partial z$ and total velocity $u_t = u$. These equations are subject to the following boundary conditions:

$y = 0$	$u = v = 0$	$w_z = 0$	$(\partial H / \partial y)_w = 0$	(21a)
$y = \delta$	$u = u_e(x,z)$	$w_z = w_{ze}$	$H = H_e$	(21b)

The infinite swept wing equations are obtained by neglecting the spanwise variation of u, v, w and H. They are given by:

Continuity

$$\frac{\partial}{\partial x} (\rho u h_2 \sin\theta) + \frac{\partial}{\partial y} (\overline{\rho v} h_1 h_2 \sin\theta) = 0 \qquad (22)$$

x-Momentum

$$\rho \frac{u}{h_1} \frac{\partial u}{\partial x} + \overline{\rho v} \frac{\partial u}{\partial y} - \rho \cot\theta \, K_1 u^2 + \rho \csc\theta \, K_2 w^2 + \rho K_{12} u w$$
$$= \rho_e \left(\frac{u_e}{h_1} \frac{\partial u_e}{\partial x} - \cot\theta \, K_1 u_e^2 + \csc\theta \, K_2 w_e^2 + K_{12} u_e w_e \right) + \frac{\partial}{\partial y} \left(\mu \frac{\partial u}{\partial y} - \rho \overline{u'v'} \right)$$
$$(23)$$

z-Momentum

$$\rho \frac{u}{h_1} \frac{\partial w}{\partial x} + \overline{\rho v} \frac{\partial w}{\partial y} - \rho \cot\theta \, K_2 w^2 + \rho \csc\theta \, K_1 u^2 + \rho K_{21} u w$$
$$= \rho_e \left(\frac{u_e}{h_1} \frac{\partial w_e}{\partial x} - \cot\theta \, K_2 w_e^2 + \csc\theta \, K_1 u_e^2 + K_{21} u_e w_e \right) + \frac{\partial}{\partial y} \left(\mu \frac{\partial w}{\partial y} - \rho \overline{w'v'} \right)$$
$$(24)$$

Energy

$$\rho \, \frac{u}{h_1} \, \frac{\partial H}{\partial x} + \overline{\rho v} \, \frac{\partial H}{\partial y} = \frac{\partial}{\partial y} \left[\frac{\mu}{Pr} \, \frac{\partial H}{\partial y} + \mu \left(1 - \frac{1}{Pr} \right) \frac{\partial}{\partial y} \left(\frac{u_t^2}{2} \right) - \rho \overline{v'H'} \right] \tag{25}$$

The boundary conditions are the same as those given by (11) except that u_e and w_e are independent of z.

CLOSURE ASSUMPTIONS FOR THE REYNOLDS STRESSES

For turbulent flows, it is necessary to make closure assumptions for the Reynolds stresses, $-\rho\overline{u'v'}$, $-\rho\overline{w'v'}$ and $-\rho\overline{v'H'}$. In the study reported here we satisfy the closure conditions by using the eddy-diffusivity concept and relate the Reynolds stresses to the mean velocity and total enthalpy profiles by

$$-\rho\overline{u'v'} = \rho\varepsilon_m \frac{\partial u}{\partial y} \quad , \quad -\rho\overline{w'v'} = \rho\varepsilon_m \frac{\partial w}{\partial y} \qquad (26a)$$

$$-\rho\overline{v'H'} = \rho\varepsilon_H \frac{\partial H}{\partial y} \qquad (26b)$$

By means of "turbulent" Prandtl number, $Pr_t (\equiv \varepsilon_m/\varepsilon_H)$, we can also write (26b) as

$$-\rho\overline{v'H'} = \rho\frac{\varepsilon_m}{Pr_t}\frac{\partial H}{\partial y} \qquad (26c)$$

We use the eddy-viscosity formulation of reference [10], and define ε_m by two separate formulas. In the so-called *inner region of the boundary layer,* (ε_m) is defined by the following formula

$$(\varepsilon_m)_i = L^2\left[\left(\frac{\partial u}{\partial y}\right)^2 + \left(\frac{\partial w}{\partial y}\right)^2 + 2\cos\theta\left(\frac{\partial u}{\partial y}\right)\left(\frac{\partial w}{\partial y}\right)\right]^{1/2} \qquad (27)$$

where

$$L = 0.4y[1 - \exp(-y/A)] \qquad (28a)$$

$$A = 26\frac{\nu}{u_\tau}\left(\frac{\rho}{\rho_w}\right)^{1/2} \quad , \qquad u_\tau = \left(\frac{\tau_{tw}}{\rho_w}\right)^{1/2} \qquad (28b)$$

$$\tau_{tw} = \mu_w\left[\left(\frac{\partial u}{\partial y}\right)_w^2 + \left(\frac{\partial w}{\partial y}\right)_w^2 + 2\cos\theta\left(\frac{\partial u}{\partial y}\right)_w\left(\frac{\partial w}{\partial y}\right)_w\right]^{1/2} \qquad (28c)$$

In the outer region ε_m is defined by the following formula

$$(\dot\varepsilon_m)_o = 0.0168\left|\int_0^\infty (u_{te} - u_t)dy\right| \qquad (29)$$

13

where

$$u_{te} = (u_e^2 + w_e^2 + 2u_e w_e \cos\theta)^{1/2} \qquad (30a)$$

$$u_t = (u^2 + w^2 + 2uw \cos\theta)^{1/2} \qquad (30b)$$

The inner and outer regions are established by the continuity of the eddy-viscosity formula.

According to a number of studies, the turbulent Prandtl number is relatively constant across the boundary layer (see reference [14], for example). In our study, we shall take it equal to 0.90.

TRANSFORMATION OF THE GOVERNING EQUATIONS

The boundary-layer equations can be solved when they are expressed either in physical coordinates or in transformed coordinates. Each coordinate has its own advantages. In three-dimensional flows, where the computer storage and time becomes quite important, the choice of using transformed coordinates becomes necessary as well as convenient because the transformed coordinates allow large steps to be taken in the streamwise and spanwise directions. In addition, they remove the singularity the equations have in physical coordinates at $x = 0$ and $z = 0$.

Let us consider the transformation of the equations given by (1) to (4). In this case we first define the transformed coordinates by

$$x = x, \quad z = z, \quad d\eta = \left(\frac{u_e}{\rho_e \mu_e s_1}\right)^{1/2} \rho \, dy, \quad s_1 = \int_0^x h_1 \, dx \tag{31}$$

and introduce a two-component vector potential such that

$$\rho u h_2 \sin\theta = \frac{\partial \psi}{\partial y}, \quad \rho w h_1 \sin\theta = \frac{\partial \phi}{\partial y}$$

$$\overline{\rho v} h_1 h_2 \sin\theta = -\left(\frac{\partial \psi}{\partial x} + \frac{\partial \phi}{\partial z}\right) \tag{32}$$

In addition, we define dimensionless ψ and ϕ by

$$\psi = (\rho_e \mu_e u_e s_1)^{1/2} h_2 \sin\theta \, f(x,z,\eta)$$

$$\phi = (\rho_e \mu_e u_e s_1)^{1/2} u_{ref}/u_e \, h_1 \sin\theta \, g(x,z,\eta) \tag{33}$$

Using these transformations and the relations given by (9), (10) and (26a,c), after some rearranging, we get

x-Momentum

$$(bf'')' + m_1 ff'' - m_2 (f')^2 - m_5 f'g' + m_6 f''g - m_8 (g')^2 + m_{11} c$$

$$= m_{10}\left(f' \frac{\partial f'}{\partial x} - f'' \frac{\partial f}{\partial x}\right) + m_7\left(g' \frac{\partial f'}{\partial z} - f'' \frac{\partial g}{\partial z}\right) \tag{34}$$

z-Momentum

$$(bg'')' + m_1 fg'' - m_4 f'g' - m_3(g')^2 + m_6 gg'' - m_9(f')^2 + m_{12}c$$

$$= m_{10} \left(f' \frac{\partial g'}{\partial x} - g'' \frac{\partial f}{\partial x} \right) + m_7 \left(g' \frac{\partial g'}{\partial z} - g'' \frac{\partial g}{\partial z} \right) \qquad (35)$$

Energy

$$(\mu_1 E')' + \mu_2 E' + \mu_3' = m_{10} \left(f' \frac{\partial E}{\partial x} - E' \frac{\partial f}{\partial x} \right) + m_7 \left(g' \frac{\partial E}{\partial z} - E' \frac{\partial g}{\partial z} \right) \qquad (36)$$

Here primes denote differentiation with respect to η and

$$f' = u/u_e, \qquad\qquad g' = w/u_{ref}, \qquad\qquad E = H/H_e \qquad (37a)$$

$$b = C(1 + \epsilon_m^+), \qquad C = \frac{\rho\mu}{\rho_e \mu_e}, \qquad c = \frac{\rho_e}{\rho}, \qquad \epsilon_m^+ = \epsilon_m/\nu \qquad (37b)$$

The coefficients m_1 to m_{12}, μ_1 to μ_3 are given by

$$m_1 = \frac{1}{2} \left(1 + \frac{s_1}{h_1 u_e} \frac{\partial u_e}{\partial x} \right) + \frac{s_1 (\rho_e \mu_e)^{-1/2}}{h_1 h_2 \sin\theta} \frac{\partial}{\partial x} (h_2 \sin\theta \sqrt{\rho_e \mu_e})$$

$$m_2 = \frac{s_1}{h_1 u_e} \frac{\partial u_e}{\partial x} - s_1 K_1 \cot\theta$$

$$m_3 = -s_1 \cot\theta\, K_2 \frac{u_{ref}}{u_e}$$

$$m_4 = s_1 K_{21}, \qquad m_5 = \frac{s_1}{h_2} \frac{u_{ref}}{u_e^2} \frac{\partial u_e}{\partial z} + K_{12} s_1 \frac{u_{ref}}{u_e} \qquad (38)$$

$$m_6 = \frac{s_1}{h_1} \left(\sqrt{\rho_e \mu_e u_e s_1}\, h_2 \sin\theta \right)^{-1} \frac{\partial}{\partial z} \left(\sqrt{\rho_e \mu_e u_e s_1}\, h_1 \sin\theta \frac{u_{ref}}{u_e} \right)$$

$$m_7 = \frac{s_1}{h_2} \frac{u_{ref}}{u_e}, \qquad m_8 = s_1 K_2 \csc\theta \left(\frac{u_{ref}}{u_e} \right)^2, \qquad m_9 = s_1 K_1 \csc\theta \frac{u_e}{u_{ref}}$$

$$m_{10} = \frac{s_1}{h_1},$$

$$m_{11} = s_1 \left[\frac{1}{u_e h_1} \frac{\partial u_e}{\partial x} + \frac{w_e}{u_e^2 h_2} \frac{\partial u_e}{\partial z} - \cot\theta\, K_1 + \csc\theta\, K_2 \left(\frac{w_e}{u_e} \right)^2 + K_{12} \frac{w_e}{u_e} \right]$$

16

$$m_{12} = \frac{s_1}{u_e u_{ref}} \left(\frac{u_e}{h_1} \frac{\partial w_e}{\partial x} + \frac{w_e}{h_2} \frac{\partial w_e}{\partial z} - \cot\theta \, K_2 w_e^2 + \csc\theta \, K_1 u_e^2 + K_{21} w_e u_e \right) \quad (38)$$

$$\mu_1 = \frac{C}{Pr} \left(1 + \varepsilon_m^+ \frac{Pr}{Pr_t} \right), \quad \mu_2 = m_1 f + m_6 g,$$

$$\mu_3 = C \frac{u_e^2}{H_e} \left(1 - \frac{1}{Pr} \right) \left[f'f'' + g'g'' \left(\frac{u_{ref}}{u_e} \right)^2 + \frac{u_{ref}}{u_e} \cos\theta \, (f'g'' + g'f'') \right] \quad (39)$$

To transform the governing stagnation-line equations, we define the transformed coordinates by

$$x = x, \qquad z = z, \qquad d\eta = \left(\frac{u_{xe}}{\rho_e \mu_e h_1} \right)^{1/2} \rho dy \quad (40)$$

the two-component vector potential by

$$\rho u_x h_2 \sin\theta = \frac{\partial \psi}{\partial y}, \quad \rho w h_1 \sin\theta = \frac{\partial \phi}{\partial y}$$

$$\overline{\rho v} h_1 h_2 \sin\theta = -\left(\psi + \frac{\partial \phi}{\partial z} \right) \quad (41)$$

and the dimensionless ψ and ϕ by

$$\psi = (\rho_e \mu_e u_{xe} h_1)^{1/2} h_2 \sin\theta \, f(z,\eta)$$

$$\phi = (\rho_e \mu_e u_{xe} h_1)^{1/2} h_1 \sin\theta \, \frac{u_{ref}}{u_{xe}} g(z,\eta) \quad (42)$$

With these new variables, for laminar flows $(b \equiv C)$, the stagnation-line equations can be written as

x-Momentum

$$(bf'')' + ff'' - (f')^2 - m_5 f'g' + m_6 f''g + m_{11}c = m_7 \left(g' \frac{\partial f'}{\partial z} - f'' \frac{\partial g}{\partial z} \right) \quad (43)$$

z-Momentum

$$(bg'')' + fg'' - m_3(g')^2 + m_6 gg'' + m_{12}c = m_7 \left(g' \frac{\partial g'}{\partial z} - g'' \frac{\partial g}{\partial z} \right) \quad (44)$$

17

Energy

$$(\mu_1 E')' + \mu_2 E' + \mu_3' = m_7 \left(g' \frac{\partial E}{\partial z} - E' \frac{\partial g}{\partial z} \right) \tag{45}$$

Here m_3, m_5, m_6, m_{11} and m_{12} are:

$$m_3 = -h_1 K_2 \cot\theta \ \frac{u_{ref}}{u_{xe}}$$

$$m_5 = h_1 \frac{u_{ref}}{u_{xe}} \left(K_{12} + \frac{h_2^{-1}}{u_{xe}} \frac{\partial u_{xe}}{\partial z} \right)$$

$$m_6 = [(\rho_e \mu_e u_{xe} h_1)^{1/2} h_2 \sin\theta]^{-1} \frac{\partial}{\partial z} \left[\sqrt{\rho_e \mu_e u_{xe} h_1} \ h_1 \sin\theta \ \frac{u_{ref}}{u_{xe}} \right] \tag{46}$$

$$m_7 = \frac{h_1}{h_2} \frac{u_{ref}}{u_{xe}}$$

$$m_{11} = 1 + \frac{h_1}{h_2} \frac{w_e}{u_{xe}^2} \frac{\partial u_{xe}}{\partial z} + h_1 \frac{w_e}{u_{xe}} K_{12}$$

$$m_{12} = \frac{h_1}{h_2} \frac{w_e}{u_{xe} u_{ref}} \frac{\partial w_e}{\partial z} - \frac{h_1 \cot\theta \ K_2 w_e^2}{u_{xe} u_{ref}}$$

The coefficients μ_1, μ_2, μ_3 are:

$$\mu_1 = \frac{C}{Pr} \ , \qquad \mu_2 = f + m_6 g \ , \qquad \mu_3 = \frac{C}{H_e} \left(1 - \frac{1}{Pr} \right) u_{ref}^2 \ g' g'' \tag{47}$$

To transform the governing infinite-swept-wing equations, we use the transformation given by (31) to (33) and write (23) to (25) as:

x-Momentum

$$(bf'')' + m_1 ff'' - m_2 (f')^2 - m_5 f'g' - m_8 (g')^2 + m_{11} c$$
$$= \frac{s_1}{h_1} \left(f' \frac{\partial f'}{\partial x} - f'' \frac{\partial f}{\partial x} \right) \tag{48}$$

18

z-Momentum

$$(bg'')' + m_1 fg'' - m_4 f'g' - m_3(g')^2 - m_9(f')^2 + m_{12}c$$
$$= \frac{s_1}{h_1}\left(f'\ \frac{\partial g'}{\partial x} - g''\ \frac{\partial f}{\partial x}\right) \tag{49}$$

The energy equation is the same as the energy equation for the general case, (36), except that the right-side of (36) is:

$$= \frac{s_1}{h_1}\left(f'\ \frac{\partial E}{\partial x} - E'\ \frac{\partial f}{\partial x}\right) \tag{50}$$

The coefficients μ_1 and μ_3 remain unchanged. However, μ_2 now becomes equal to $m_1 f$.

The definitions of the coefficients m_1 to m_{12} in (48) and (49) are the same as those in (38) except now

$$m_5 = K_{12}s_1\ \frac{u_{ref}}{u_e}$$

$$m_6 = 0$$

$$m_{11} = s_1\left[\frac{1}{u_e h_1}\ \frac{\partial u_e}{\partial x} - \cot\theta\ K_1 + \csc\theta\ K_2\left(\frac{w_e}{u_e}\right)^2 + K_{12}\ \frac{w_e}{u_e}\right] \tag{51}$$

$$m_{12} = \frac{s_1}{u_e u_{ref}}\left(\frac{u_e}{h_1}\ \frac{\partial w_e}{\partial x} - \cot\theta\ K_2 w_e^2 + \csc\theta\ K_1 u_e^2 + K_{21}w_e u_e\right)$$

To transform the governing chordwise attachment-line equations we use the transformed coordinates given by (31) and define the two-component vector potential by

$$\rho\ uh_2\ \sin\theta = \frac{\partial\psi}{\partial y}\ ,\qquad w_z\rho h_1\ \sin\theta = \frac{\partial\phi}{\partial y}$$

$$\overline{\rho v}h_1 h_2\ \sin\theta = -\left(\frac{\partial\psi}{\partial x} + \phi\right) \tag{52}$$

with ψ and ϕ still given by (33). With these variables, and with the relations given by (26a,c), the <u>chordwise attachment-line equations</u> can be written as

19

x-Momentum

$$(bf'')' + m_1 ff'' - m_2(f')^2 + m_6 f''g + m_{11}c$$
$$= \frac{s_1}{h_1}\left(f'\frac{\partial f'}{\partial x} - f''\frac{\partial f}{\partial x}\right) \qquad (53)$$

z-Momentum

$$(bg'')' + m_1 fg'' - m_4 f'g' - m_3(g')^2 + m_6 gg'' - m_9(f')^2 + m_{12}c$$
$$= \frac{s_1}{h_1}\left(f'\frac{\partial g'}{\partial x} - g''\frac{\partial f}{\partial x}\right) \qquad (54)$$

The definitions of the coefficients m_1 to m_{12} in (53) and (54) are the same as those in (38) except now

$$m_3 = \frac{s_1}{h_2}\frac{u_{ref}}{u_e}$$

$$m_6 = m_3$$

$$m_9 = 0 \qquad\qquad\qquad (55a)$$

$$m_{11} = \frac{s_1}{h_1}\frac{1}{u_e}\frac{\partial u_e}{\partial x} - s_1 \cot\theta \; K_1$$

$$m_{12} = \frac{s_1}{u_{ref}}\left(\frac{1}{h_1}\frac{\partial w_{ze}}{\partial x} + \frac{w_{ze}^2}{u_e h_2} + K_{21}w_{ze}\right)$$

The energy equation is the same as the energy equation for the general case (36), except that the right side of (36) is the same as (50); the coefficients μ_1 and μ_2 remain the same but now

$$\mu_3 = \frac{Cu_{ref}^2}{H_e}\left(1 - \frac{1}{Pr}\right)f'f'' \qquad (55b)$$

The general boundary conditions for the governing three-dimensional boundary-layer equations are:

$$\eta = 0 \qquad\qquad f_w = f'_w = g_w = g'_w = 0, \qquad\qquad E'_w = 0 \qquad (56a)$$

$$\eta = \eta_\infty \qquad\qquad f' = 1, \quad g' = w_e/u_{ref} \qquad\qquad E = 1 \qquad (56b)$$

Those equations (56) apply to the general case, to the stagnation-line equations, to the infinite-swept-wing equations as well as to the chordwise attachment-line equations, except, however, that the edge boundary condition (g' at $\eta = \eta_\infty$) is different for the chordwise-attachment-line equations; it is given by $g' = w_{ze}/u_{ref}$.

Eddy Viscosity Equations

If we apply the transformation given by (31) to (33) to the eddy-viscosity formulas given by (27) to (30), we get

$$(\epsilon_m^+)_i = \left(\frac{\nu_e}{\nu}\right) Re^{1/2} \frac{1}{c}\left(0.4 \int_0^\eta c d\eta\right)^2 \left[1 - \exp\left(-\frac{y}{A}\right)\right]^2$$

$$\left[(f'')^2 + \left(\frac{u_{ref}}{u_e}\right)^2 (g'')^2 + 2\cos\theta \; \frac{u_{ref}}{u_e} f''g''\right]^{1/2}$$

$$(57)$$

$$(\epsilon_m^+)_o = \left(\frac{\nu_e}{\nu}\right) Re^{1/2}(0.0168) \int_0^\eta c \left\{\left[1 + \left(\frac{w_e}{u_e}\right)^2 + 2\left(\frac{w_e}{u_e}\right)\cos\theta\right]^{1/2}\right.$$

$$\left. - \left[(f')^2 + \left(\frac{u_{ref}}{u_e}\right)^2 (g')^2 + 2 \; \frac{u_{ref}}{u_e}\cos\theta \; f'g'\right]\right\}d\eta$$

$$(58)$$

Here $Re = u_e s_1/\nu_e$ and

$$\frac{y}{A} = \frac{\nu_e}{\nu} \frac{1}{26} Re^{1/4}\left(\int_0^\eta c d\eta\right) c_w^{1/2} c^{1/2} \left[(f_w'')^2 + \left(\frac{u_{ref}}{u_e}\right)^2 (g_w'')^2 + 2\cos\theta \; \frac{u_{ref}}{u_e} f_w''g_w''\right]^{1/4}$$

$$(59)$$

NUMERICAL METHOD

We use the Box method to solve the governing equations. This is a two-point finite-difference method that has successfully been applied to two-dimensional flows by Keller and Cebeci and to three-dimensional flows by Cebeci. A detailed description of the method is presented in References [11] and [14]. For this reason only a brief description of it will be presented here.

One of the basic ideas of the Box method is to write the governing system of equations in the form of a first-order system. Thus, in our case, the first derivatives of f, g and E with respect to η are introduced as new unknown functions. With the resulting first-order system and an arbitrary rectangular net, we use simple centered difference quotients and averages at the midpoints of net rectangles and net segments to get second-order accurate finite-difference equations. Then nonlinear difference equations are linearized by using Newton's method and the resulting linear system is solved by the block-elimination method discussed by Isaacson and Keller [17].

Numerical Formulation of the Momentum Equations

In our present method we solve the two momentum equations simultaneously. Essentially the stagnation-line equations, infinite-swept-wing equations and the chordwise attachment-line equations are two-dimensional flow equations in the sense that these equations have two independent variables, (x, η) or (z, η). On the other hand, the two momentum equations (34) and (35) are three-dimensional flow equations for obvious reasons. The solution of the two-dimensional flow equations is discussed in considerable length in references [11], [14], [18]; for this reason we shall only discuss the solution of three-dimensional-flow equations, namely, (34), (35) and their boundary conditions, (56).

With the introduction of new independent variables $u(x,z,\eta)$, $v(x,z,\eta)$, $w(x,z,\eta)$ and $t(x,z,\eta)$, the equations given by (34) and (35) can be written as

$$f' = u \tag{60a}$$

$$u' = v \tag{60b}$$

22

$$g' = w \qquad \qquad (60c)$$

$$w' = t \qquad \qquad (60d)$$

$$(bv)' + m_1 fv - m_2 u^2 - m_5 uw + m_6 vg - m_7 w^2 + m_{11}c = m_{10}\left(u\,\frac{\partial u}{\partial x} - v\,\frac{\partial f}{\partial x}\right)$$

$$+ m_7\left(w\,\frac{\partial u}{\partial z} - v\,\frac{\partial g}{\partial z}\right) \qquad (60e)$$

$$(bt)' + m_1 ft - m_4 uw - m_3 w^2 + m_6 gt - m_9 u^2 + m_{12}c = m_{10}\left(u\,\frac{\partial w}{\partial x} - t\,\frac{\partial f}{\partial x}\right)$$

$$+ m_7\left(w\,\frac{\partial w}{\partial z} - t\,\frac{\partial g}{\partial z}\right) \qquad (60f)$$

We next consider the net cube shown in Figure 7 and introduce the net points by

$$x_0 = 0 \qquad\qquad x_n = x_{n-1} + k_n \qquad\qquad n = 1,2, \ldots, N$$

$$z_0 = 0 \qquad\qquad z_i = z_{i-1} + r_i \qquad\qquad i = 1,2, \ldots, I \qquad (61)$$

$$\eta_0 = 0 \qquad\qquad \eta_j = {}_{j-1} + h_j \qquad\qquad j = 1,2, \ldots, J$$

Figure 7. Net cube for the difference equations for three-dimensional flows.

23

The difference equations which are to approximate (60a) to (60d) are obtained by averaging about the midpoint $(x_n, z_j, n_{j-1/2})$

$$\frac{f_j^{n,i} - f_{j-1}^{n,i}}{h_j} = u_{j-1/2}^{n,i} \tag{62a}$$

$$\frac{u_j^{n,i} - u_{j-1}^{n,i}}{h_j} = v_{j-1/2}^{n,i} \tag{62b}$$

$$\frac{g_j^{n,i} - g_{j-1}^{n,i}}{h_j} = w_{j-1/2}^{n,i} \tag{62c}$$

$$\frac{w_j^{n,i} - w_{j-1}^{n,i}}{h_j} = t_{j-1/2}^{n,i} \tag{62d}$$

where, for example,

$$u_{j-1/2}^{n,i} = \frac{1}{2}(u_j^{n,i} + u_{j-1}^{n,i})$$

The difference equations which are to approximate (60e,f) are rather lengthy. To illustrate the difference equations to equations similar to (60e,f), we consider the following model equation:

$$v' + m_1 fv = m_{10} u \frac{\partial u}{\partial x} + m_7 w \frac{\partial u}{\partial z} \tag{63}$$

The difference equations for this equation are

$$\frac{\bar{v}_j - \bar{v}_{j-1}}{h_j} + (m_1)_{i-1/2}^{n-1/2}(\bar{f}\bar{v})_{j-1/2} = (m_{10})_{i-1/2}^{n-1/2} \bar{u}_{j-1/2}\left(\frac{\bar{u}_n - \bar{u}_{n-1}}{k_n}\right)$$
$$+ (m_7)_{i-1/2}^{n-1/2}\bar{w}_{j-1/2}\left(\frac{\bar{u}_i - \bar{u}_{i-1}}{r_i}\right) \tag{64}$$

where, for example,

$$\bar{v}_j = \frac{1}{4}(v_j^{n,i} + v_j^{n,i-1} + v_j^{n-1,i-1} + v_j^{n-1,i})$$

$$\bar{u}_n = \frac{1}{4}(u_j^{n,i} + u_j^{n,i-1} + u_{j-1}^{n,i} + u_{j-1}^{n,i-1})$$

24

$$\bar{u}_i = \frac{1}{4} \left(u_j^{n,i} + u_j^{n-1,i} + u_{j-1}^{n,i} + u_{j-1}^{n-1,i} \right)$$

$$(m_1)_{i-1/2}^{n-1/2} = \frac{1}{4} \left[(m_1)_i^n + (m_1)_{i-1}^n + (m_1)_i^{n-1} + (m_1)_{i-1}^{n-1} \right]$$

The boundary conditions for the system of equations given by (56) at $x = x_n$ and at $z = z_i$ are:

$$f_0^{n,i} = 0, \quad g_0^{n,i} = 0, \quad u_0^{n,i} = 0, \quad w_0^{n,i} = 0, \quad u_J^{n,i} = 1, \quad w_J^{n,i} = \left(\frac{w_e}{u_{ref}} \right)^{n,i}$$

(65)

If we assume $(f_j^{n-1,i-1}, u_j^{n-1,i-1}, v_j^{n-1,i-1}, g_j^{n-1,i-1}, w_j^{n-1,i-1}, t_j^{n-1,i-1})$, $(f_j^{n,i-1}, u_j^{n,i-1}, v_j^{n,i-1}, g_j^{n,i-1}, w_j^{n,i-1}, t_j^{n,i-1})$, and $(f_j^{n-1,i}, u_j^{n-1,i}, v_j^{n-1,i}, g_j^{n-1,i}, w_j^{n-1,i}, t_j^{n-1,i})$ to be known for $0 \leq j \leq J$, then the difference equations (62) and the difference equations for (60e,f) along with (65) yield an implicit nonlinear algebraic system of $6J + 6$ equations in as many unknowns $(f_j^n, u_j^n, v_j^n, g_j^n, w_j^n, t_j^n)$. We solve this nonlinear system by means of Newton's method. The resulting linearized system is then solved by using the block elimination method discussed by Isaacson and Keller [17].

Numerical Formulation of the Energy Equation

The numerical formulation of the energy equation is very similar to the formulation described for the momentum equations. To reduce (36) to a first-order system, we introduce a new independent variable $G(x,z,\eta)$ and write (36) as

$$E' = G \tag{66a}$$

$$(\mu_1 G)' + \mu_2 G + \mu_3' = m_{10} \left(u \frac{\partial E}{\partial x} - G \frac{\partial f}{\partial x} \right) + m_7 \left(w \frac{\partial E}{\partial z} - G \frac{\partial g}{\partial z} \right) \tag{66b}$$

The difference equation for (66) is written again by averaging about the midpoint $(x_n, z_i, \eta_{j-1/2})$, similar to those given by (62). The difference equation for (66b) is written similar to (64). The boundary conditions in (56) for the energy equation are:

$$G_0^{n,i} = 0 \quad , \quad E_J^{n,i} = 1 \tag{67}$$

The resulting algebraic system of $2J = 2$ equations in as many unknowns (E_j^n, G_j^n), which is linear, is directly solved by the block elimination method.

RESULTS AND DISCUSSION

General Discussion of the Method and the Solution Procedure

The present method is a very general boundary-layer method for three-dimensional flows. For a given pressure distribution, boundary-layer calculations can be done for infinite-swept wings or finite wings. The pressure distribution can be either experimental or theoretical. When it is experimental, we use the approximate procedure described in Appendix A to get the velocity components from the experimental pressure distribution.

The boundary-layer calculations can be started either at the stagnation line or at some specified percent chord away from the stagnation line. The initial conditions on the root section can be started by using either the infinite swept wing assumptions or the chordwise attachment-line equations. Sometimes, as shall be described later, it is necessary to prescribe the initial conditions at the tip section. In such a case, we use the infinite swept wing equations, which, as previously discussed, are an approximation to the flow in this region.

The present boundary-layer method uses a body-oriented nonorthogonal coordinate system. A separate program is used to calculate the coordinate system and its geometric parameters such as the geodesic-curvature-parameters K_1, K_2, K_{12}, K_{21} and the metric coefficients h_1, h_2. This is discussed in detail in Appendix B.

In the present program for a given spanwise station we march in the streamwise direction. Since the linearized form of the equations are being solved, we iterate at each x-station until some convergence criterion is satisfied. For both laminar and turbulent flows we use the wall shear parameter f_w'' as the convergence criterion. Laminar flow calculations are stopped when
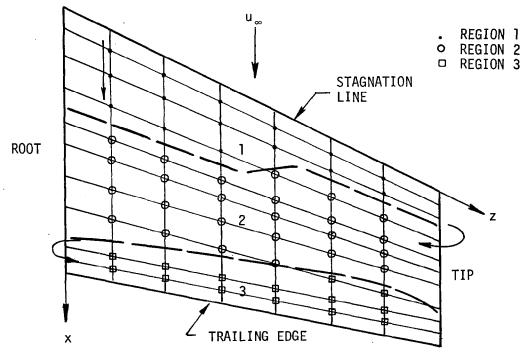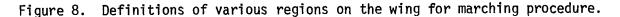
$$\left| \delta f_w'' \right| < \delta_1$$

where the value of δ_1 is prescribed. A typical value of δ_1 is 10^{-4}. For turbulent flows, the convergence criterion is slightly different; it is given by

$$\left| \frac{\delta f_w''}{f_w'' + \delta f_w''/2} \right| < \delta_2$$

where a typical value of δ_2 is 10^{-2}.

Whether the initial calculations start at the root section or at the tip section is determined by the sign of the external spanwise velocity component w_e. To illustrate our marching procedure, let us assume that the wing has three regions defined by the sign of w_e. In region 1, w_e is positive; in region 2, w_e is negative; and in region 3, w_e is positive (see figure 8). Let us also assume that region 1 starts from the leading edge. In this case, our calculations start at the root section. At the leading edge we use the stagnation-line equations for one x-station and switch to either chordwise attachment-line equations (if $w \equiv 0$) or to the infinite swept-wing equations. With either one of these equations we march in the streamwise

Figure 8. Definitions of various regions on the wing for marching procedure.

28

direction to the net point before w_e changes sign. Then we go back to the stagnation line and after solving the stagnation-line equations, we start solving the general three-dimensional flow equations at the second x-station. This procedure is repeated as before for all stations up to and including the tip section in region 1. The calculations are continued into region 2 starting at the tip by solving the infinite swept-wing equations along the tip up to the beginning of region 3. At that time we go back to the next spanwise station of region 2 and start solving the general three-dimensional flow equations for region 2. This procedure is again repeated for region 2 up to and including the root section in region 2. The calculations at the root section are extended to region 3 by solving either the infinite-swept-wing equations or the chordwise attachment-line equations, and the procedure used for region 1 is repeated for this region.

It should be pointed out that our marching procedure utilizes the sign of w_e. It may be argued that the marching procedure should be based on the local value of w. In the calculations presented here, no difficulties were encountered when we used the above procedure including the cases where local cross-flow velocity changed sign within the boundary layer. However, this point needs further exploration.

The present method is developed in such a way that one can use non-uniform net spacings in the streamwise and in the spanwise directions. Across the layer one can either use a uniform grid or a variable grid discussed in reference [14]. According to this grid, the net in the η-direction is a geometric progression having the property that the ratio of lengths of any two adjacent intervals is a constant; that is, $h_j = Kh_{j-1}$. The distance to the j-th line is given by the following formula:

$$\eta_j = h_1(K^j - 1)/(K - 1) \qquad K > 1 \qquad (68)$$

There are two parameters: h_1, the length of the first $\Delta\eta$ step, and K, the ratio of two successive steps. The total number of points J can be calculated by the following formula:

$$J = \frac{\ln[1 + (K - 1)(n_\infty/h_1)]}{\ln K} \qquad (69)$$

For further details, see reference [14].

In the present method the pressure-gradient parameters m_1 to m_{12} are determined numerically from the given external velocity distributions u_e and w_e. For example, the derivative of du_e/dx is obtained by using three-point Lagrange interpolation formulas given by $(n < N)$

$$\frac{du_e}{dx}\bigg|_n = -\frac{u_e^{n-1}}{A_1}(x_{n+1} - x_n) + \frac{u_e^n}{A_2}(x_{n+1} - 2x_n + x_{n-1}) \qquad (70)$$
$$+ \frac{u_e^{n+1}}{A_3}(x_n - x_{n-1})$$

Here N refers to the last x^n station and

$$A_1 = (x_n - x_{n-1})(x_{n+1} - x_{n-1})$$
$$A_2 = (x_n - x_{n-1})(x_{n+1} - x_n) \qquad (71)$$
$$A_3 = (x_{n+1} - x_n)(x_{n+1} - x_{n-1})$$

The derivative of du_e/dx at the end point $n = N$ is given by

$$\frac{du_e}{dx}\bigg|_N = -\frac{u_e^{N-2}}{A_1}(x_N - x_{N-1}) - \frac{u_e^{N-1}}{A_2}(x_N - x_{N-2}) + \frac{u_e^N}{A_3}(2x_N - x_{N-2} - x_{N-1}) \qquad (72)$$

where now

$$A_1 = (x_{N-1} - x_{N-2})(x_N - x_{N-2})$$
$$A_2 = (x_{N-1} - x_{N-2})(x_N - x_{N-1}) \qquad (73)$$
$$A_3 = (x_N - x_{N-1})(x_N - x_{N-2})$$

Similar derivatives for du_e/dz, dw_e/dz, dw_e/dx can be written by slightly modifying the above equations.

Boundary-Layer Parameters

Once the solutions are obtained, we calculate the usual boundary-layer parameters, which in terms of physical variables and transformed variables for the general case are:

Chordwise local-skin-friction coefficient

$$c_{f_c} = \frac{2\tau_c}{\rho_\infty u_\infty^2} = \frac{2(\tau_x + \tau_z \cos\theta)}{\rho_\infty u_\infty^2}$$

$$= \frac{2C_w}{\sqrt{R_s}} \left(\frac{\rho_e}{\rho_\infty}\right)\left[\left(\frac{u_e}{u_\infty}\right)^2 f_w'' + \frac{u_e u_{ref}}{u_\infty^2} \cos\theta\ g_w''\right] \tag{74}$$

Spanwise local-skin-friction coefficient

$$c_{f_n} = \frac{2\tau_z \sin\theta}{\rho_\infty u_\infty^2} = \frac{2C_w}{\sqrt{R_s}} \left(\frac{\rho_e}{\rho_\infty}\right)\left(\frac{u_e u_{ref}}{u_\infty^2}\right) \sin\theta\ g_w'' \tag{75}$$

Cross-flow angle

$$\beta = \tan^{-1}\left(\frac{c_{f_n}}{c_{f_c}}\right) \tag{76}$$

Chordwise displacement thickness

$$\delta_c^* = \int_0^\infty \left(1 - \frac{\rho}{\rho_e}\frac{\bar{u}}{\bar{u}_e}\right)dy = \frac{s_1}{\sqrt{R_s}}\left[I_\rho - \frac{(f_\infty + u_{ref}/u_e \cos\theta\ g_\infty)}{(1 + w_e/u_e \cos\theta)}\right] \tag{77}$$

Spanwise displacement thickness

$$\delta_n^* = \int_0^\infty \left(1 - \frac{\rho}{\rho_e}\frac{\bar{w}}{\bar{w}_e}\right)dy = \frac{s_1}{\sqrt{R_s}}\left(I_\rho - \frac{u_{ref}}{w_e}g_\infty\right) \tag{78}$$

Chordwise momentum thickness θ_c

$$\theta_c = \int_0^\infty \frac{\rho \bar{u}}{\rho_e \bar{u}_e}\left(1 - \frac{\bar{u}}{\bar{u}_e}\right)dy = \frac{s_1}{\sqrt{R_s}}\left[\frac{(f_\infty + u_{ref}/u_e \cos\theta \; g_\infty)}{(1 + w_e/u_e \cos\theta)}\right.$$

$$\left. - \int_0^\infty \frac{(f' + u_{ref}/u_e \cos\theta \; g')^2}{(1 + w_e/u_e \cos\theta)^2} \, d\eta \right] \tag{79}$$

Spanwise momentum thickness θ_n

$$\theta_n = \int_0^\infty \frac{\rho \bar{w}}{\rho_e \bar{w}_e}\left(1 - \frac{\bar{w}}{\bar{w}_e}\right)dy = \frac{s_1}{\sqrt{R_s}}\left(\frac{u_{ref}}{w_e}\right)\left[g_\infty - \frac{u_{ref}}{w_e}\int_0^\infty (g')^2 d\eta\right] \tag{80}$$

Here

$$R_s = \frac{u_e s_1}{\nu_e} \quad , \qquad I_\rho = \int_0^\infty \frac{\rho_e}{\rho} \, d\eta \tag{81}$$

and $\bar{u}/\bar{u}_e$ and $\bar{w}/\bar{w}_e$ are the chordwise and spanwise velocity components given by

$$\frac{\bar{u}}{\bar{u}_e} = \frac{u + w \cos\theta}{u_e + w_e \cos\theta} = \frac{f' + (u_{ref}/u_e)g' \cos\theta}{1 + w_e/u_e \cos\theta} \tag{82}$$

$$\frac{\bar{w}}{\bar{w}_e} = \frac{w \sin\theta}{w_e \sin\theta} = \frac{u_{ref}}{w_e}\frac{w}{u_{ref}} = \frac{u_{ref}}{w_e} g' \tag{83}$$

On the plane of symmetry these boundary-layer parameters are defined by:

$$c_{f_c} = \frac{2\tau_x}{\rho_\infty u_\infty^2} = \frac{2C_w}{\sqrt{R_s}}\left(\frac{\rho_e}{\rho_\infty}\right)\left(\frac{u_e}{u_\infty}\right)^2 f_w'' \tag{84}$$

$$c_{f_n} = \delta_n^* = \theta_n = 0 \tag{85}$$

$$\delta_c^* = \int_0^\infty \left(1 - \frac{\rho u}{\rho_e u_e}\right)dy = \frac{s_1}{\sqrt{R_s}}(I_\rho - f_\infty) \tag{86}$$

32

$$\theta_c = \int_0^\infty \frac{\rho u}{\rho_e u_e}\left(1 - \frac{u}{u_e}\right)dy = \frac{S_1}{\sqrt{R_s}}\left[f_\infty - \int_0^\infty (f')^2 d\eta\right] \qquad (87)$$

On the stagnation line they are:

$$c_{f_c} = \delta_c^* = \theta_c = 0 \qquad (88)$$

$$c_{f_n} = \frac{2\tau_z}{\rho_\infty u_\infty^2} = \frac{2C_w}{\sqrt{u_{xe} h_1/\nu_e}}\left(\frac{u_{ref} u_{xe}}{u_\infty^2}\right)\sin\theta\, g_w'' \qquad (89)$$

$$\delta_n^* = \int_0^\infty \left(1 - \frac{\rho}{\rho_e}\frac{w}{w_e}\right)dy = \sqrt{\frac{h_1 \nu_e}{u_e}}\left(I_\rho - \frac{u_{ref}}{w_e}g_\infty\right) \qquad (90)$$

$$\theta_n = \int_0^\infty \frac{\rho w}{\rho_e w_e}\left(1 - \frac{w}{w_e}\right)dy = \sqrt{\frac{h_1 \nu_e}{u_{xe}}}\frac{u_{ref}}{w_e}\left[g_\infty - \left(\frac{u_{ref}}{w_e}\right)\int_0^\infty (g')^2 d\eta\right] \qquad (91)$$

Results for Laminar Flows

To test our code for laminar incompressible flows, we have considered a test case computed earlier by Cebeci [12], by using another computer program. This test case consists of a three-dimensional laminar flow past a flat plate with attached cylinder (see figure 9). For this flow the inviscid velocity distribution is given by

$$u_e = u_\infty\left(1 + a^2\frac{\Delta_2}{\Delta_1^2}\right), \qquad w_e = -2u_\infty a^2\frac{\Delta_3}{\Delta_1^2} \qquad (92)$$

where

$$\Delta_1 = (x - x_0)^2 + z^2, \qquad \Delta_2 = -(x - x_0)^2 + z^2, \qquad \Delta_3 = (x - x_0)z \qquad (93)$$

Here u_∞ is a reference velocity, a is the cylinder radius, and x_0 denotes the distance of the cylinder axis from the leading edge $x = 0$.

Figure 9. Flow past a flat plate with attached cylinder.

The calculations were made for a Cartesian orthogonal system with u_∞ = 3050 cm/sec, a = 6.1 cm, x_0 = 45.7 cm for several x and z-stations. The present results with those of reference [12] are shown in Table 1. Note that the pressure-gradient parameters in the present method are obtained numerically, whereas in the method used in reference [12], they were obtained analytically. As can be seen from the results, there is essentially no difference between the earlier and the present results. All calculations were made with 11 points across the boundary layer and with Δx = 1.220 cm and Δz = 0.610 cm.

In Table 1 the results under the present method represent the solutions obtained by the present computer program in which the pressure-gradient parameters m_1 to m_{12} are obtained numerically from the given external velocity distribution. The results under reference [12] represent solutions obtained by another computer program to which m_1 to m_{12} are calculated analytically.

34

Table 1. Calculated Wall Shear Parameters for the Laminar
Post Problem.

x (cm)	z = 0		z = 0.610 cm	
	Present Method f''_w	Ref. [12] f''_w	Present Method f''_w	Ref. [12] f''_w
0	0.330854	0.330854	0.330854	0.330854
1.220	0.329498	0.329498	0.329461	0.329461
2.440	0.327973	0.327973	0.327711	0.327712
3.660	0.326233	0.326233	0.325852	0.325853
4.880	0.324252	0.324251	0.323584	0.323588
6.100	0.321987	0.321985	0.321103	0.321109
7.320	0.319416	0.319385	0.318078	0.318112

Results for Turbulent Flows

For turbulent flows, the accuracy of the method depends on the turbulence model as well as on the accuracy of the numerical method. According to the studies reported in references [10], [12] and [13], the present eddy-viscosity formulation gives quite satisfactory predictions for three-dimensional flows. In the studies reported here, we have considered three test cases to further test the computer program.

Test Case 1

The first test case deals with the comparison of calculated and experimental results on a swept wing for an incompressible flow. The experimental data is due to Brebner and Wyatt [19]. However, most of this data is very difficult to use for comparison purposes since the location of transition is given at one spanwise station only. Furthermore, the relatively large probe used in their experiments seems to interfere with measurements at higher angles of attack. The "good" data is near mid-semispan of the 45-degree swept wing which has a 50.8 cm constant chord and an RAE 101 section with a thickness to chord ratio of 0.12. It has no twist and has an aspect ratio of 5. The tests were conducted in RAE Bedford Low Speed Wind Tunnel at a nominal free-stream velocity of 61 meters per second, corresponding to a streamwise chord Reynolds number of 2.1 x 10^6.

For the data of Brebner and Wyatt we have made two different sets of calculations by using the infinite swept wing approximations for the external flow. With this assumption the external velocity components can be calculated exactly from the experimental pressure distribution. The first set of calculations are for an orthogonal system. For the external $\bar{u}_e(x)$ distribution shown in figure 10 with $\bar{w}_e$ = 43 m/sec, the solutions were started as laminar at the stagnation point with the stagnation-line equations and were continued with the infinite swept-wing equations up to the transition location, which according to the experimental data, was specified at $(\bar{x}/c)$ = 0.35. At that location, the turbulent flow calculations were started and were continued up to the trailing edge. At the next spanwise station, the calculations were done for full three-dimensional flows. Overall, 30 x-stations, 15 for laminar flow and 15 for turbulent flows and 3 z-stations were used. The variable grid parameters were h_1 = 0.01, K = 1.26, n_∞ = 31 yielding 30 points across the boundary layer at the trailing edge.

Figures 11 and 12 show the results. Figure 11 compares the experimental and calculated total velocity profiles at two measured x-stations, namely, at $(\bar{x}/c)$ = 0.80 and 0.98. Figure 12 shows a comparison of calculated and experimental cross-flow angle β, calculated from

$$\beta = \tan^{-1}\left(\frac{\bar{w}}{\bar{u}}\right) - \left(\frac{\pi}{2} - \epsilon\right) \tag{94a}$$

At the wall β is calculated from

$$\beta = \tan^{-1}\left(\frac{\partial \bar{w}}{\partial y}\right)_w \left(\frac{\partial \bar{u}}{\partial y}\right)_w^{-1} - \left(\frac{\pi}{2} - \theta\right) \tag{94b}$$

The second set of calculations were made for a nonorthogonal system with h_1 = 0.05, K = 1.3, n_∞ = 69 yielding 24 points across the boundary layer at the trailing edge. For the specified airfoil section, the geometric parameters were determined by using the procedure described in Appendix B and the velocity components u_e and w_e were determined (see figure 13) from the experimental pressure distribution by using the procedure described in Appendix A.

We note that in this case we have two regions of positive w_e separated by one region of negative w_e as shown schematically in figure 8. For this
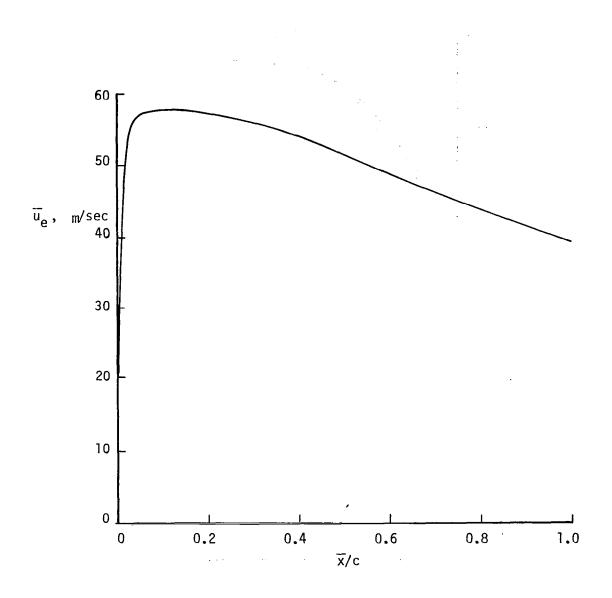
36

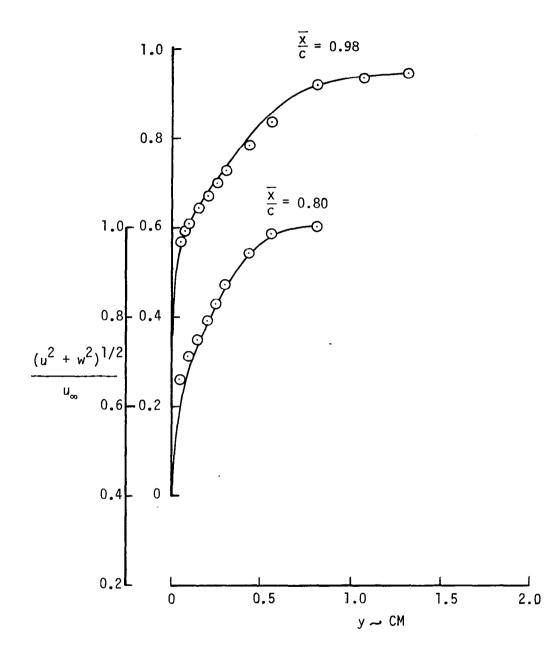Figure 10. Experimental velocity distribution for the data of Brebner and Wyatt, orthogonal system.

Figure 11. Comparison of calculated and experimental velocity profiles for the data of Brebner and Wyatt, orthogonal system.
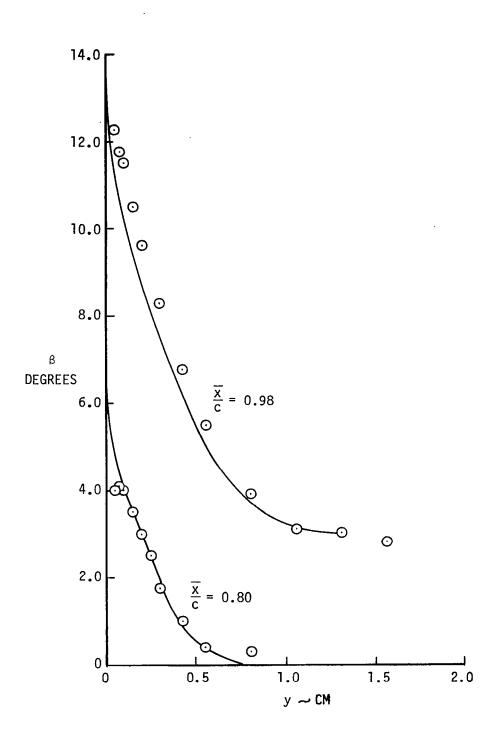
Figure 12. Comparison of calculated and experimental cross-flow-angle-distribution for the data of Brebner and Wyatt, orthogonal system.
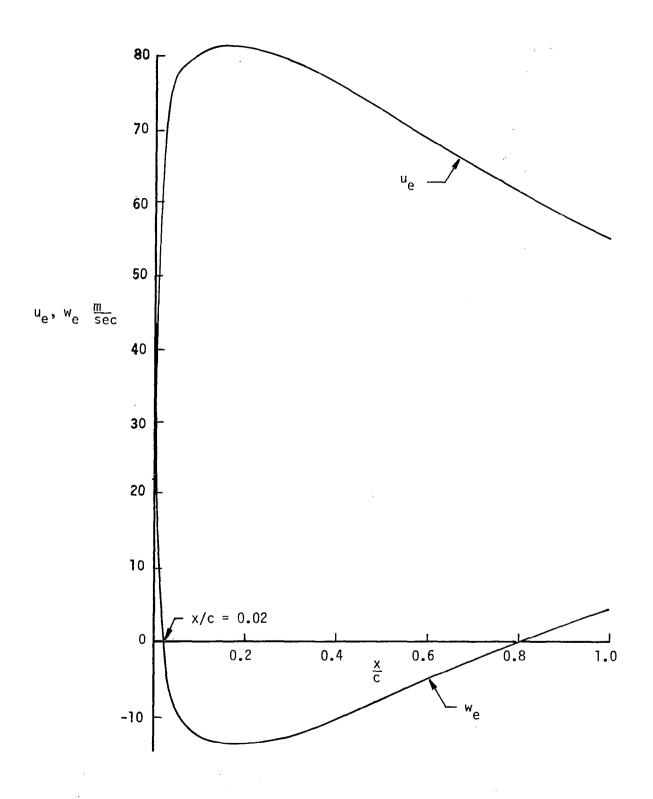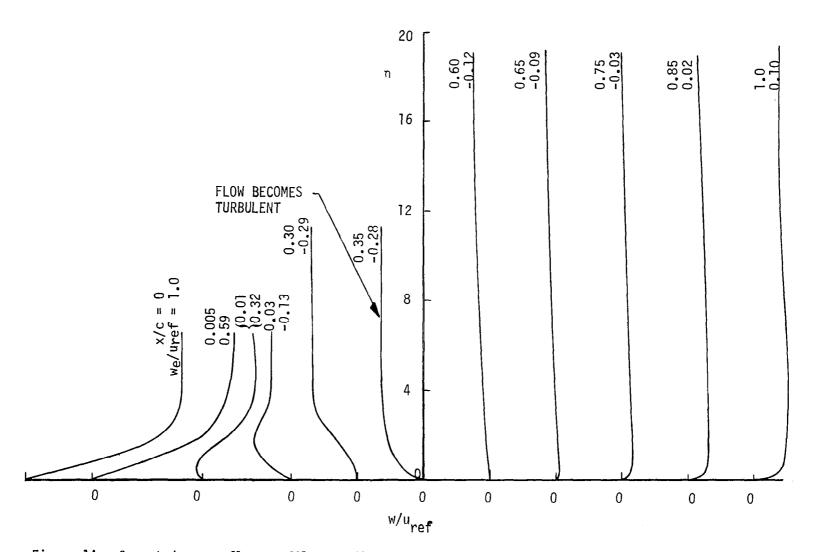
Figure 13. Experimental velocity distribution for the data of Brebner and Wyatt, nonorthogonal system.

Figure 14. Computed cross-flow profiles at different chordwise stations for the data of Brebner and Wyatt, nonorthogonal system, $u_{ref} = w_e$ at $x = 0$.

reason, the calculations were started at the stagnation line of the root
section and the marching procedure described earlier was used to compute the
flow field for three spanwise stations consisting of thirty streamwise stations.
Region 1 is a very small region, whereas region 2 is a very large region.
Figure 14 shows the variation of the cross-flow velocity across the boundary
layer for various x-stations. It is interesting to note that during the march-
ing procedure the solutions converge very fast, show no numerical problems
and all the computed velocity profiles, when rotated to the orthogonal coord-
inate system, agree extremely well with those results obtained for an ortho-
gonal system. If we use bars to denote the velocity profiles in the orthogonal
coordinate system, then the velocity profiles in the orthogonal system can be
obtained from those in the nonorthogonal system by the following formulas
given previously (see figure 6), that is,

$$\bar{u} = u \sin\theta \qquad\qquad (95a)$$

$$\bar{w} = w + u \cos\theta \qquad\qquad (95b)$$

If we denote the dimensionless stream function in the nonorthogonal system by
f and its derivatives with respect to η, then the dimensionless stream-
function in the orthogonal system F and its derivatives are related to f
and its derivatives by

$$F' = f' \qquad\qquad (96)$$

$$F'' = f'' \sqrt{\frac{\bar{x}}{\sin\theta \, s_1}}$$

Similarly,

$$G' = g' \left(\frac{u_{ref}}{\bar{w}_e}\right) + f' \frac{u_e}{\bar{w}_e} \cot\theta$$

$$G'' = \left[g'' \left(\frac{u_{ref}}{\bar{w}_e}\right) + f'' \left(\frac{\bar{u}_e}{\bar{w}_e}\right) \cot\theta \right] \sqrt{\frac{1}{\sin\theta} \frac{\bar{x}}{s_1}} \qquad\qquad (97)$$

Test Case 2

The second test case is an incompressible flow past an untapered,
untwisted, 30 degrees-swept-wing having NACA 0012 streamwise airfoil sections.
Its semispan is 2.78 meters and its chord is 1.15 meters. The inviscid velocity

42

distribution was obtained by using Hess's potential flow method [20] for an angle of attack of 8 degrees, giving a lift coefficient of 0.51. A total of 16 chordwise strips on the semispan were taken and each strip was subdivided into 50 elements. Because the calculated inviscid surface velocities are given in terms of their Cartesian components, additional calculations were made to put these velocities into the nonorthogonal coordinate system. Calculations were made only for the lower surface of the wing for a chord Reynolds number of $R_c = 5.88 \times 10^6$.

The external velocity distribution for this wing is quite interesting in that, except for a very small region, all the external spanwise velocity components w_e are positive (see figure 15). Figure 16 shows the computed chordwise local skin-friction coefficients and displacement thicknesses at various spanwise stations. According to our marching procedure, the solutions start at the root section by using the stagnation-line equations at $x/c = 0$ and by using the infinite swept wing equations at $x/c > 0$. With transition specified at $(x/c) = 0.02$, the calculations continue up to the trailing edge since w_e is positive for all chordwise stations. The procedure is repeated for the next spanwise station, NZ = 2. The procedure at NZ = 3, 4, 5 and 6 are different. Since, at some chordwise stations, w_e becomes negative, the solutions that originate from the stagnation line at a given spanwise station $3 \le NZ \le 6$, continue up to the last chordwise station where w_e is positive, say $(x/c)_0$, and then go back to the stagnation line. At NZ = 7, the procedure used for NZ = 3, 4, 5, 6 is repeated for the same chordwise stations. At $(x/c) > (x/c)_0$, however, they continue up to the trailing edge by using the infinite swept wing equations. At $8 \le NZ \le 22$, the procedure used at NZ = 2 is repeated. In this way all the chordwise stations for the spanwise stations NZ = 1, 2, 7 to 22 are completed. To complete the rest of the chordwise stations for NZ = 3, 4, 5 and 6 we go back to NZ = 6 and by using the infinite swept wing equations, we start marching at $(x/c) > (x/c)_0$ up to the last (x/c) station, say $(x/c)_1$, where w_e is negative. Then we go back to NZ = 5, 4, 3 and repeat the same procedure, but this time using the general three-dimensional flow equations. At NZ = 3, we turn back. By using the infinite swept wing equations, we start marching at $(x/c) > (x/c)_1$. Then we go to the next spanwise stations
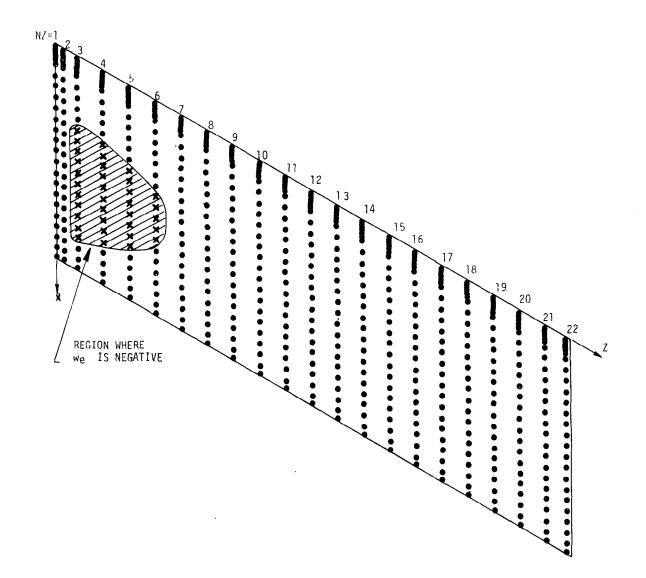
Figure 15. The wing for test case 2. The symbols denote the stations where the boundary-layer calculations are made. Dots correspond to stations were w_e is positive and x's correspond to negative w_e.
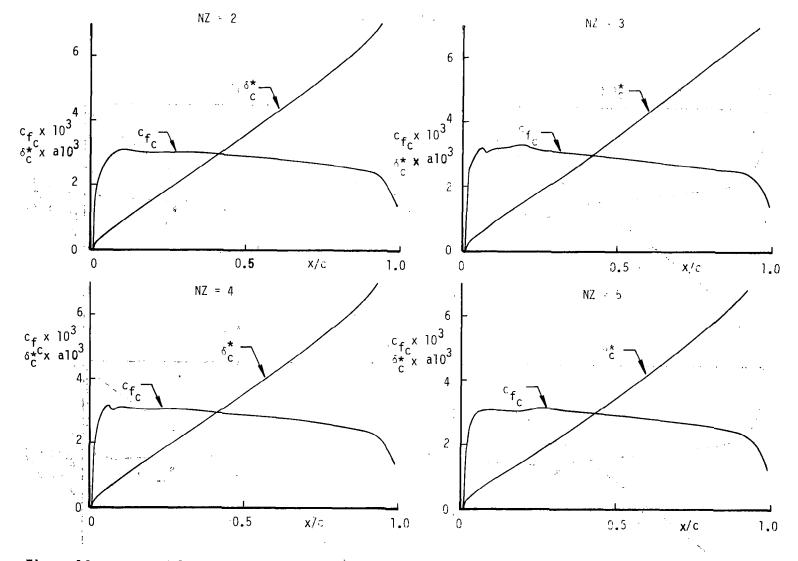
Figure 16. Computed lower surface chordwise local skin-friction coefficients and displacement thickness at various spanwise stations for test case 2. Note that the solutions start at the stagnation line which is at x/c = 0.01, a = 1.0 (ft), a = 0.305 (meters)
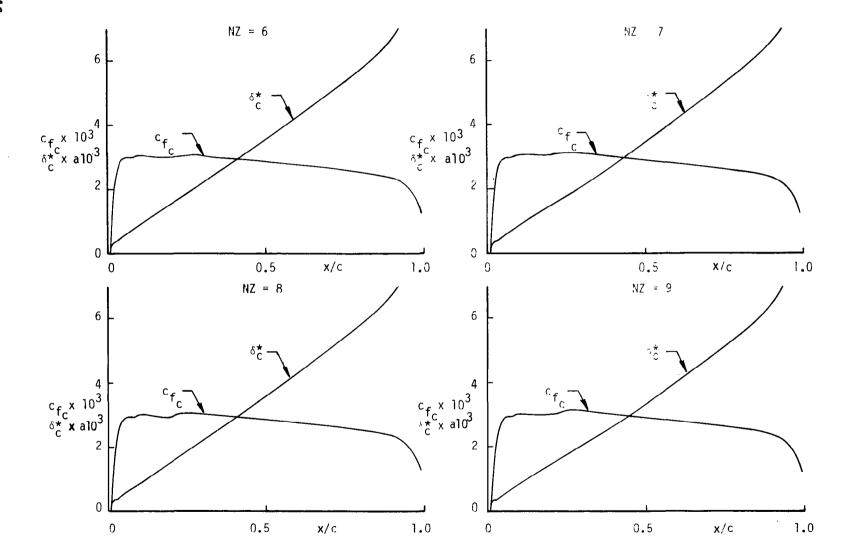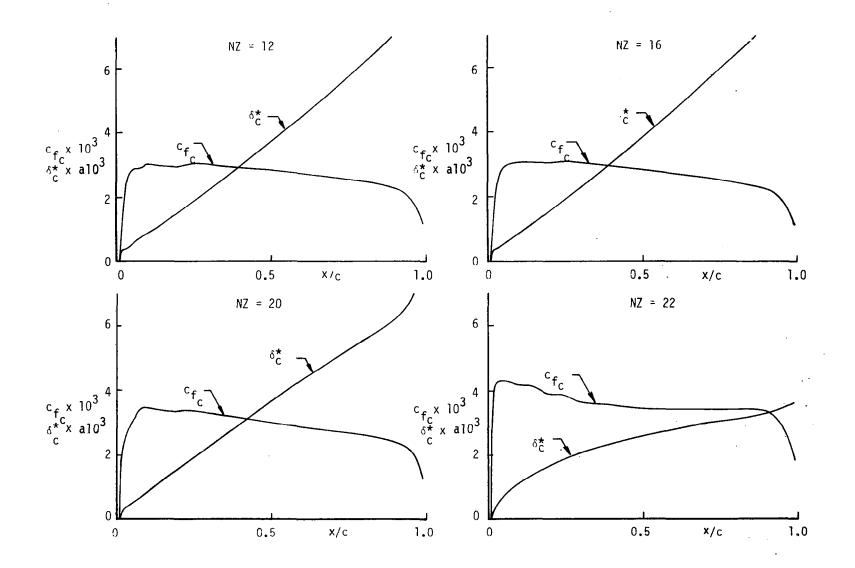
Figure 16.   Continued.

Figure 16. Concluded.

NZ = 3, 4, and 5, and repeat this procedure with the general three-dimensional flow equations, thus completing the calculation over the entire wing surface.

Test Case 3

The first two test cases considered for turbulent flows were for incompressible flows. The third test case is for compressible flows. The wing selected for this case has a planform and dimensions similar to that given in figure 4 of [6], except that its trailing edge is straight. It is given below as figure 17. Also, in our system the wing root is at $\overline{y}$ = 0.76 meters corresponding to the z = 0 degree plane in [6]. The wing has a 5.6-meter root-chord, 1.02 meter tip chord; the tip is at $\overline{y}$ = 7.1 meters. Thickness is added by supercritical airfoils of 12.38-percent thickness at the root, and 9.24-percent thickness at the tip with parabolic variation inbetween. Twist was generated by a linear

Figure 17. The planform for test case 3. Dashed lines denote the modified planform for our calculations.

variation of the trailing-edge height over the $\overline{x},\overline{y}$-plane, with the leading edge of the wing remaining on the $\overline{x},\overline{y}$-plane over its entire length. Total twist variation between the root and the tip is 6 degrees.

The calculations were made for the upper surface at Mach numbers of M = 0.5 and 0.99 by using the experimental pressure distributions given in [21] as Table III-230 and Table III-28, respectively. The external velocity components were obtained by using the procedure described in Appendix A and by using the velocity program described in Appendix C. Since the experimental pressure distribution does not extend over the entire chord-length, the boundary-layer calculations were started at x/c = 0.025 and were continued up to (x/c) = 0.975. The transition point was assumed at (x/c) = 0.10. The unit Reynolds number in both cases was 4.9×10^6. The spanwise extent of calculation is from $\overline{y}$ = 0.76 meters to $\overline{y}$ = 6.6 meters and was again limited by the available pressure measurements. For this reason we have extrapolated the experimental data to get the data on the root section. For both cases, w_e was negative on the entire wing; as a result calculations were started at the tip section and were continued all the way to the root section. Note that in terms of the spanwise boundary-layer coordinate z, $\overline{y}$ = 0.76 meters corresponds to z = 0, and $\overline{y}$ = 6.6 meters corresponds to z = 0.92.

The computed chordwise and spanwise values of c_f and δ^* are shown for both cases in figures 18 to 23. Note that for M_∞ = 0.50, the chordwise local skin-friction distribution at z = 0.76 is quite different from those c_f-distributions at z = 0.52 and 0.28. Similarly, the chordwise variation of displacement thickness for the same Mach number at each spanwise station are quite different from each other. The large variation in both skin-friction and displacement thickness distributions in spanwise direction is partially due to the experimental pressure distribution selected for this sample calculation. That is, the flow was obviously separated on the outboard panels of the wing, and it was the separated flow pressure distribution which was specified for boundary-layer calculations. For M_∞ = 0.99, the chordwise local skin-friction and the displacement thickness distributions for three different spanwise stations are qualitatively similar, as one would expect them to be for properly designed wing with attached flow.
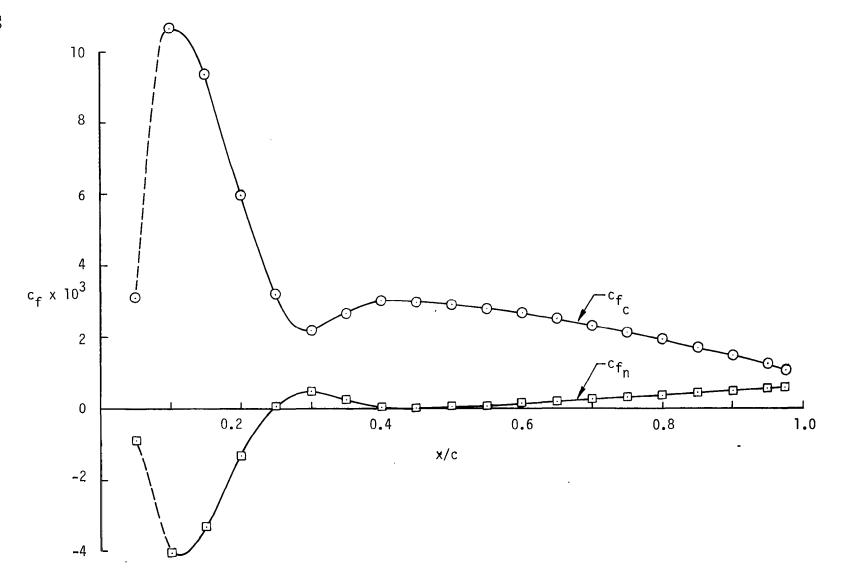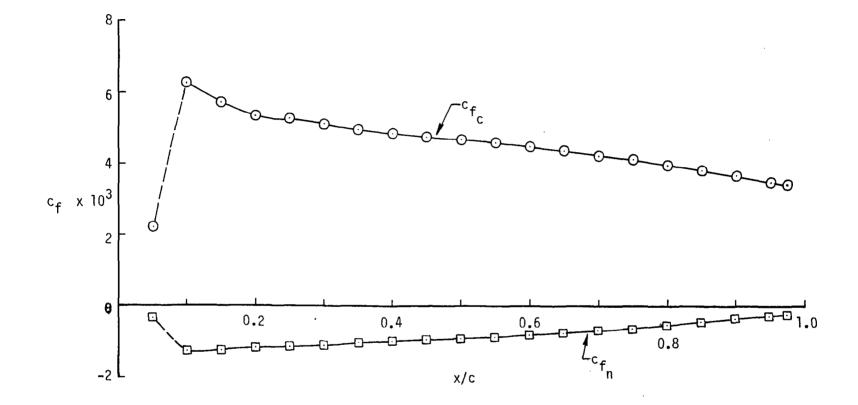
$c_f \times 10^3$

10

8

6

4

2

0

-2

-4

c_{f_c}

c_{f_n}

0.2   0.4   0.6   0.8   1.0

x/c

Figure 18. Variation of the local skin-friction in the chordwise direction for $M_\infty = 0.50$. (a) z = 0.76. The dashed lines denote the laminar flow solutions and the solid lines denote the turbulent flow solutions.

Figure 18. (b) z = 0.52.

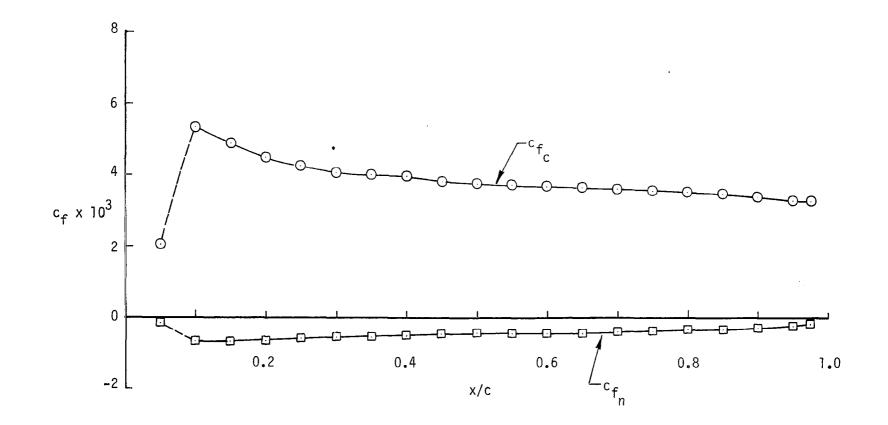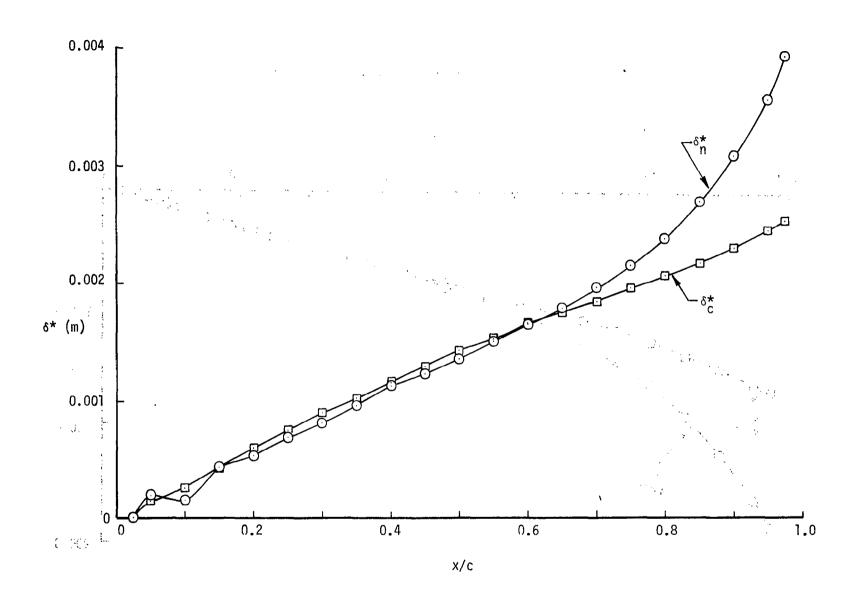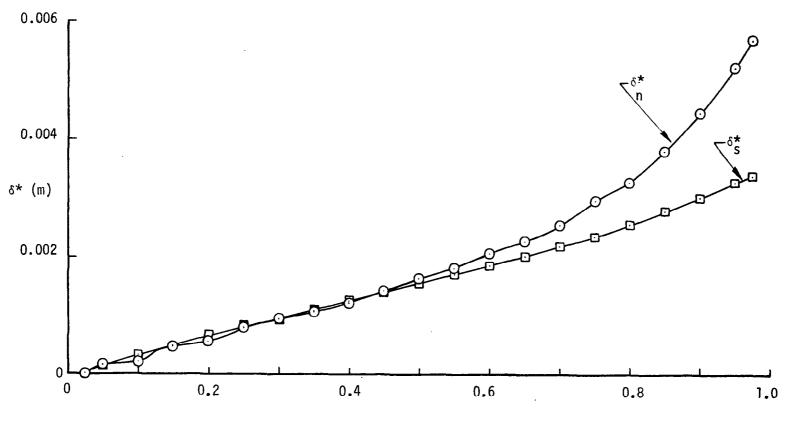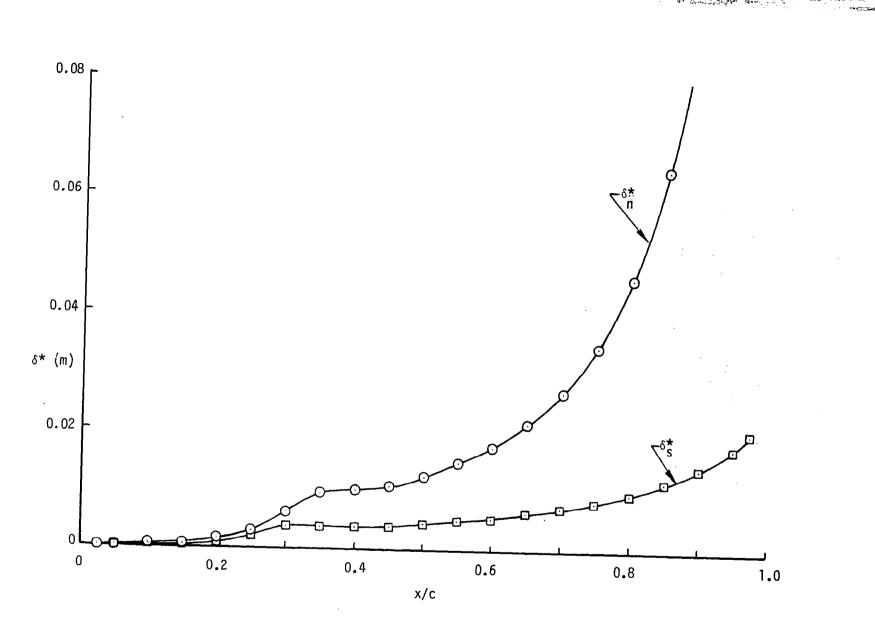Figure 18. (c) z = 0.28.

Figure 19. Variation of the displacement thickness in the chordwise direction for $M_\infty = 0.50$.
(a) $z = 0.76$.

Figure 19.   (b)   z = 0.52.
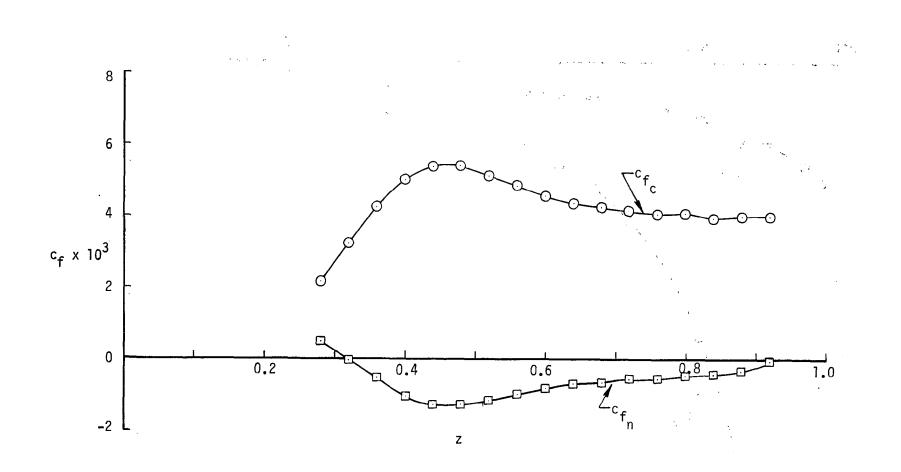
Figure 19. (c) z = 0.28.

Figure 20. Variation of the local skin-friction in the spanwise direction for $M_\infty = 0.50$.
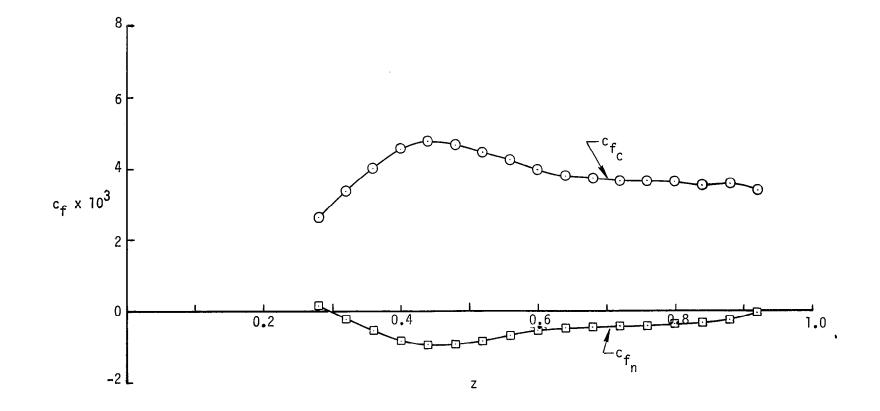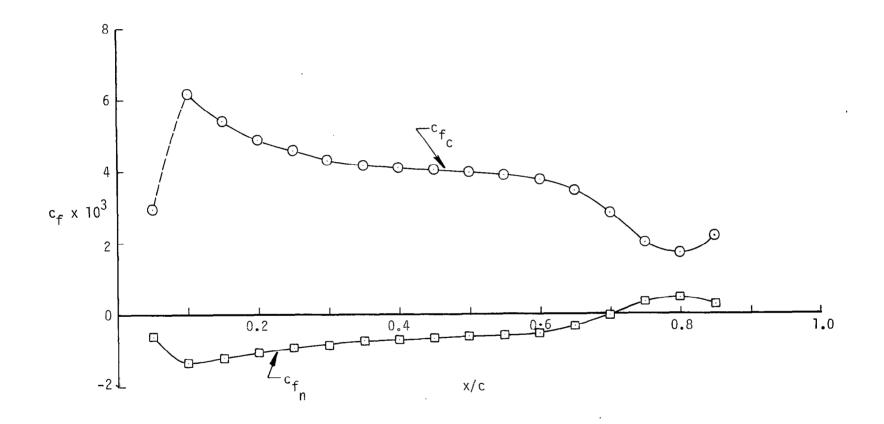   (a) x/c = 0.30.

Figure 20. (b) x/c = 0.60

Figure 21. Variation of the local skin-friction in the chordwise direction for $M_\infty = 0.99$.
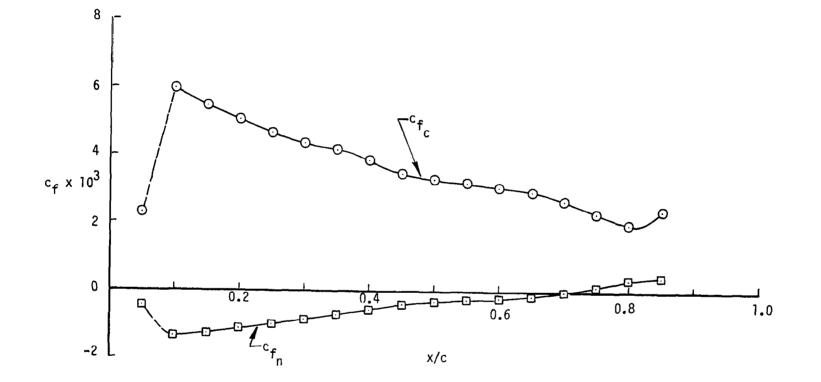(a) z = 0.76.

Figure 21. (b) z = 0.52.

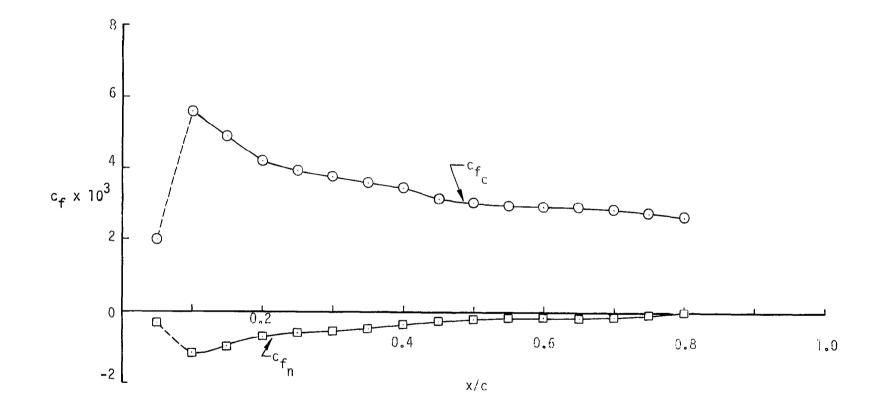Figure 21. (c) z = 0.28.
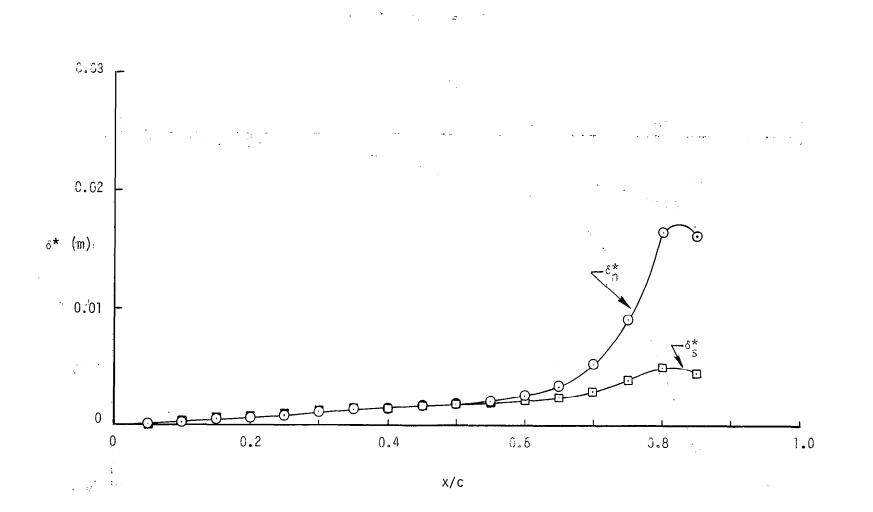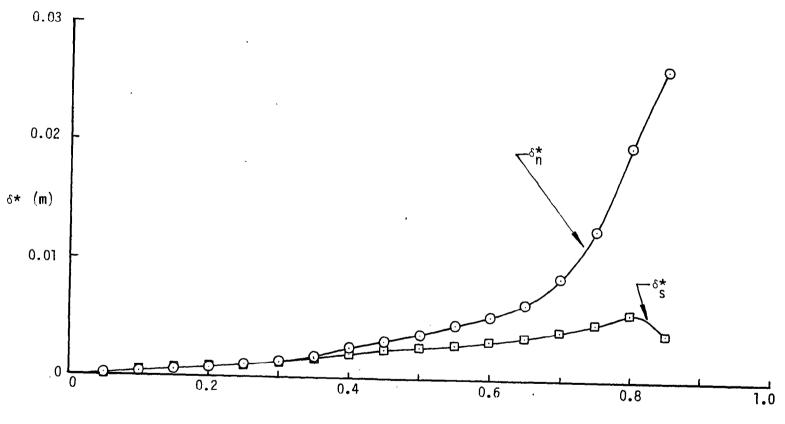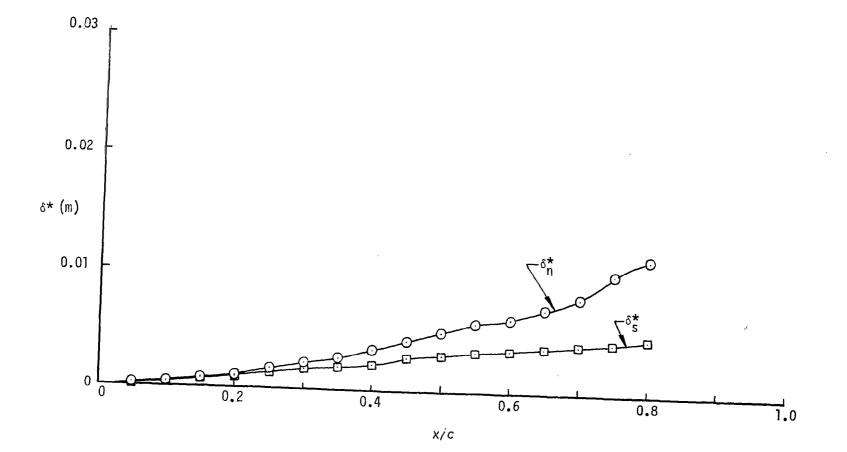
Figure 22. Variation of the displacement thickness in the chordwise direction for $M_\infty = 0.99$.
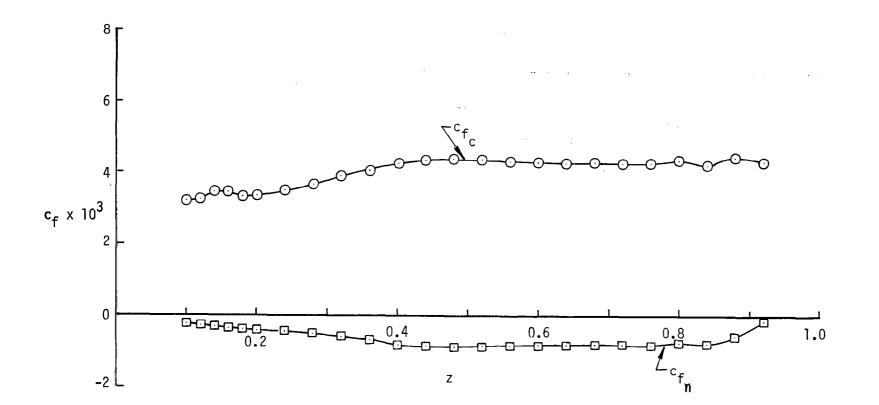(a) z = 0.76.

Figure 22. (b) z = 0.52.

Figure 22. (c) z = 0.28.

Figure 23. Variation of the local skin friction in the spanwise direction for $M_\infty = 0.99$.
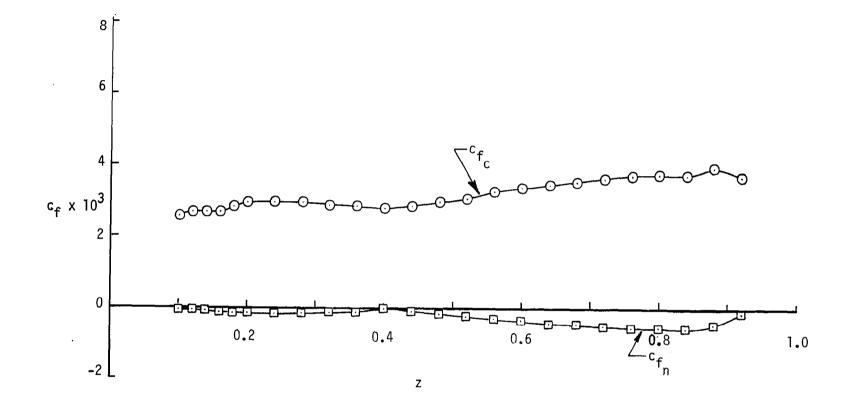(a) x/c = 0.30.

Figure 23. (b) x/c = 0.60.

CONCLUDING REMARKS

According to the studies presented in this report, the three-dimensional boundary layers on swept wings can be computed very effectively by our method. The geometry package represents the wing analytically and accounts for its geometric parameters. However, the method should be tested further and additional capabilities should be added in order to make the method more versatile. In particular:

1. The marching procedure should be further tested. Although the sample calculations are very encouraging, additional test cases must be made for different pressure distributions on different wings to check the numerical calculations for strong negative cross-flow velocity profiles.

2. The present procedure to calculate the attachment-line flow near the wing leading edge should be modified to handle cases where the attachment streamline deviates considerably from a constant chordwise location along the span.

3. The boundary-layer method should be coupled to an inviscid code so that inviscid flow and viscous flow calculations can be made at the same time.

APPENDIX A

CALCULATION OF THE EXTERNAL VELOCITY COMPONENTS
FROM A GIVEN PRESSURE DISTRIBUTION

Because the experimental pressure distribution is very seldom given with sufficient accuracy or in sufficient detail to calculate the inviscid velocity components from Euler's equations, we resort to the local sweep theory. The local sweep theory is known to give reasonable results when applied to regions of high aspect ratio wings that are outside the influence of root and tip effects. If the spanwise pressure gradient is weak, as on the midportion of a swept wing, the accuracy of the approximate method is almost exact. In regions of root and tip influence a correction to the local sweep theory is applied in order to account for the effective reduction of the sweep angle. Our procedure is explained below.

Consider the resultant velocity vector $\vec{u}_s$ in the tangent plane at a point P on the wing surface (figure A1). The basic assumption for the local sweep theory is that projections of both the freestream velocity vector $\vec{u}_\infty$ and the local velocity vector $\vec{u}_s$ upon the z-axis are equal, or

$$u_p = u_s \sin\beta = u_\infty \sin\lambda \tag{A1}$$

Here λ is the local sweep angle obtained from

$$\lambda = \pi - \cos^{-1}\left(\vec{t}_2 \cdot \frac{\vec{u}_\infty}{u_\infty}\right) \tag{A2}$$

From the parallelogram law for the addition of vector components we obtain

$$\frac{u_e}{u_\infty} = \frac{u_s \cos\beta}{u_\infty \sin\theta} \tag{A3}$$

$$\frac{w_e}{u_\infty} = \frac{u_s}{u_\infty}\left(\frac{\sin\beta \sin\theta - \cos\theta \cos\beta}{\sin\theta}\right) \tag{A4}$$

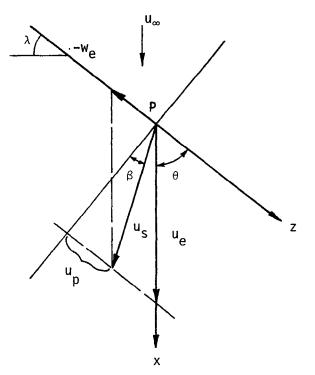Elimination of β from (A3) and (A4) gives

Figure A1. Velocity vector in the tangent plane at a point P on the wing. λ is the sweep angle.

$$\frac{u_e}{u_\infty} = \frac{\sqrt{(u_s/u_\infty)^2 - \sin^2\lambda}}{\sin\theta} \tag{A5}$$

$$\frac{w_e}{u_\infty} = \sin\lambda - \frac{u_e}{u_\infty}\cos\theta \tag{A6}$$

The total velocity ratio (u_s/u_∞) is calculated from

$$\left(\frac{u_s}{u_\infty}\right)^2 = 1 + \frac{1 - \left[P_{T_1}/P_{T_2}(1 + \gamma/2C_p M_\infty^2)\right]^{(\gamma-1)/\gamma}}{(\gamma - 1)M_\infty^2/2} \tag{A7}$$

with P_{T_1} and P_{T_2} denoting the values of total pressure before and after the shock, respectively, and C_p is the pressure coefficient, $C_p = (P - P_\infty)/(1/2\rho u_\infty^2)$. Equation (A7) is valid for an adiabatic flow through a shock wave, but since the total pressure ratio across the shock is seldom known, it is set equal to one. This approximation introduces only a few percent error into

68

the velocity calculations because the total pressure jump across a swept shock is small even for freestream Mach numbers approaching unity. The total pressure ratio must also remain close to one for the first-order boundary-layer theory to be valid in front and behind the shock wave.

Equations (A5) to (A6) are approximately valid for the root and tip regions if the local sweep angle is replaced by an effective sweep angle,

$$\lambda_e = \lambda - F_{r,t}\lambda_{r,t} \tag{A8}$$

Here λ denotes the local sweep angle, $\lambda_{r,t}$ denote the root or tip sweep angle for the given z-coordinate line. $F_{r,t}$ are the spanwise interpolation factors for the root and tip, respectively. They are given in graphical form in [10] as a function of nondimensional spanwise distance in terms of root or tip chord. The curve fit for the above interpolation factors are:

$$F_r = \frac{7}{45}\left(\frac{52}{90(\bar{y}/c_r) + 7} - 1\right) \qquad 0 \le \frac{\bar{y}}{c_r} \le 0.5 \tag{A9}$$

$$F_t = 0.1\left(\frac{0.24}{28(b - \bar{y})/c_t + 3} - 1\right) \qquad 0 \le \frac{b - \bar{y}}{c_t} \le 0.75 \tag{A10}$$

where b is the semispan, and c_r and c_t are the root chord and the tip chord, respectively. Since no overlap of (A9) and (A10) is allowed, there is a lower limit of wing aspect ratio to which the local sweep theory with correction can be applied. For example, for a wing with no taper, the wing aspect ratio must be greater than or equal to 2.5. As a consequence of the effective reduction of sweep angle, the calculation of velocity components in a nonorthogonal coordinate system must reflect the fact that the angle between the coordinate lines is effectively increased. Simple geometrical consideration of a sheared wing shows that the effective coordinate angle should be expressed as

$$\cos\theta_e = \frac{\sin\lambda_e}{\sin\theta} \cos\theta \tag{A11}$$

To use equations (A5) and (A6) near the wing root or tip λ is replaced by λ_e and θ is replaced by θ_e.

APPENDIX B

CALCULATION OF THE COORDINATE SYSTEM AND ITS GEOMETRIC PARAMETERS

Coordinate System

We assume the wing to be defined in the Cartesian coordinate system $\bar{x}, \bar{y}, \bar{z}$. Here $\bar{x}$ is in the general direction of the airplane longitudinal axis, $\bar{y}$ is in the spanwise direction and $\bar{z}$ is normal to the $\bar{x}\bar{y}$-plane. We shall also assume that the wing definition is given by a number of airfoil sections in planes $\bar{y}$ = const., which involves the specification of sets of $\bar{x}_i, \bar{z}_i$ for constant values of $\bar{y}_j$. The boundary layer is to be calculated at a fixed number of nondimensional chordwise locations $(\xi/c)_p$ for a given number of spanwise stations $\bar{y}_s$. The coordinate system for boundary-layer calculation is defined by the lines $(\xi/c)_p$ = const. and $\bar{y}_s$ = const. on the wing surface and the surface normals. Figure B1 shows the plan view of a wing with our notation. The choice of the coordinate system for boundary-layer calculations is dictated by the fact that aerodynamic data is usually given in terms of percent of chord and percent of semispan location, and by the almost uniform coverage of the wing with the chosen coordinate net.

To find the geometrical properties of the chosen coordinate lines, we need relationships between the wing defining system $\bar{x}, \bar{y}, \bar{z}$ and the surface imbedded coordinate system $(\xi/c)_p, \bar{y}_s$.

Considering $\bar{y}$ = const. planes, the following relationships hold (see Figure B2)

$$\frac{\xi}{c} = \frac{1}{c} [(\bar{x} - \bar{x}_\ell) \cos\alpha - (\bar{z} - \bar{z}_\ell) \sin\alpha] \tag{B1}$$

$$\frac{\zeta}{c} = \frac{1}{c} [(\bar{x} - \bar{x}_\ell) \sin\alpha + (\bar{z} - \bar{z}_\ell) \cos\alpha] \tag{B2}$$

where

$$c = [(\bar{x}_t - \bar{x}_\ell)^2 + (\bar{z}_t - \bar{z}_\ell)^2]^{1/2} \tag{B3}$$

$$\alpha = -\tan^{-1}\left(\frac{\bar{z}_\ell - \bar{z}_t}{\bar{x}_\ell - \bar{x}_t}\right) \tag{B4}$$

70

DEFINING AIRFOIL CROSS
SECTIONS $\bar{z}_i$, $\bar{x}_i$ FOR A
GIVEN $\bar{y}_j$

LEADING EDGE

ROOT

$\left(\dfrac{\xi}{c}\right)_p$

TIP

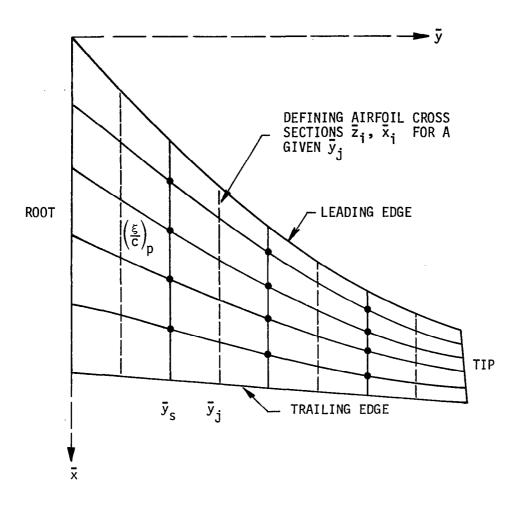$\bar{y}_s$ $\bar{y}_j$ TRAILING EDGE

$\bar{x}$

Figure B1. Plan view of a wing with our notation.

Here the subscripts ℓ and t refer to the points at the leading edge
and trailing edges, respectively,and c is the local chord length (maximum
length line).

Considering figure B2, it is obvious that (ξ/c) = const. are accept-
able coordinate lines as long as we can treat the upper and lower surfaces
separately. However, if the stagnation point s is located in the lower
surface, calculations for what we now call the upper surface contain a portion
of the lower surface and the meaning of coordinate ξ/c becomes ambiguous.
To remedy this situation and also to stretch the coordinate near the leading
edge where flow quantities vary rapidly, we employ the following transforma-
tion of the independent variable ξ/c:
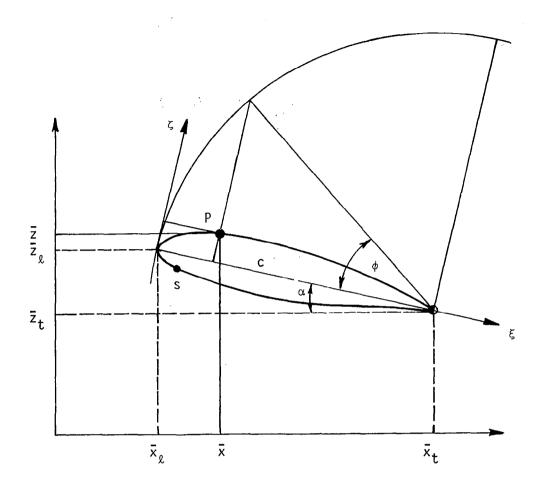
71

Figure B2. Notation for the airfoil section for a given $\bar{y}$.

$$\frac{\xi}{c} = 1 - \cos\phi \qquad\qquad (B5)$$

Here $\phi = 0$ corresponds to the leading edge, and $\phi = \pi/2$ to the trailing edge. If the upper surface is being calculated, the points on the lower surface correspond to negative values of ϕ and vice versa. On the coordinate line $\phi = $ const. we use as the independent variable the nondimensional form of $\bar{y}$ given by $y = \bar{y}/b$ where b is a scaling constant for the convenience of the user of the program. If b denotes the length of semispan, y will vary from 0 to 1. The variables ϕ, y constitute a nonorthogonal coordinate system embedded in the wing surface. It should be noted that the boundary-layer coordinates in the main text make use of a different notation, namely $x \equiv \phi$ and $z \equiv y$ in the present notation.

72

Geometric Parameters

Once the coordinate system is selected, it is necessary to calculate its geometric parameters, such as the metric coefficients, and the geodesic curvatures of the coordinate lines. In what follows we designate quantities associated with the chordwise variable with subscript one and those associated with the spanwise variable with subscript two.

The metric coefficient along a curve in space is given by

$$h^2 = \left(\frac{d\bar{x}}{dP}\right)^2 + \left(\frac{d\bar{y}}{dP}\right)^2 + \left(\frac{d\bar{z}}{dP}\right)^2 \tag{B6}$$

with P denoting a parameter. Taking $P = \phi$ along the curves $y = $ const., we can write (B6) for h_1:

$$h_1^2 = \left(\frac{\partial\bar{x}}{\partial\phi}\right)_y^2 + \left(\frac{\partial\bar{z}}{\partial\phi}\right)_y^2 \tag{B7}$$

Similarly, taking $P = y$ along the curves $\phi = $ const., we can write

$$h_2^2 = b^2 + \left(\frac{\partial\bar{x}}{\partial y}\right)_\phi^2 + \left(\frac{\partial\bar{z}}{\partial y}\right)_\phi^2 \tag{B8}$$

The derivatives in (B7) and in (B8), namely $(\partial\bar{x}/\partial\phi)_y$, $(\partial\bar{z}/\partial\phi)_y$, $(\partial\bar{x}/\partial y)_\phi$, and $(\partial\bar{z}/\partial y)_\phi$ are obtained as by-products of spline-fitting the points along the chordwise and spanwise directions at the pivotal points.

The unit tangent vector $\vec{t}$ along a curve is given by

$$\vec{t} = \frac{d\vec{r}}{ds} = \frac{d\vec{r}}{dP}\frac{1}{(ds/dP)} = \frac{1}{h}\frac{d\vec{r}}{dP} \tag{B9}$$

The unit tangent vector $\vec{t}_1$ along the curve $y = $ const. is

$$\vec{t}_1 = \frac{1}{h_1}\left[\left(\frac{\partial\bar{x}}{\partial\phi}\right)_y i + \left(\frac{\partial\bar{z}}{\partial\phi}\right)_y k\right] \tag{B10}$$

where i, j, k are unit vectors in the coordinate directions $\bar{x}, \bar{y}, \bar{z}$, respectively.

The unit tangent vector $\vec{t}_2$ along the curve ϕ = const. is

$$\vec{t}_2 = \frac{1}{h_2}\left[\left(\frac{\partial\bar{x}}{\partial y}\right)_\phi i + bj + \left(\frac{\partial\bar{z}}{\partial y}\right)_\phi k\right] \qquad (B11)$$

The angle between the coordinate lines is then

$$\cos\theta = \vec{t}_1 \cdot \vec{t}_2 = \left[\left(\frac{\partial\bar{x}}{\partial\phi}\right)\left(\frac{\partial\bar{x}}{\partial y}\right) + \left(\frac{\partial\bar{z}}{\partial\phi}\right)\left(\frac{\partial\bar{z}}{\partial y}\right)\right]/(h_1 h_2) \qquad (B12)$$

The curvature of a curve in space is given by

$$\vec{K} = \frac{d\vec{t}}{ds} = \frac{d\vec{t}}{dP}\frac{1}{(ds/dP)} = \frac{1}{h}\frac{d\vec{t}}{dP} \qquad (B13)$$

The geodesic or tangential curvature K_g of a curve on the surface can be obtained from

$$K_g = (\vec{t} \times \vec{n}) \cdot \vec{K} \qquad (B14)$$

Here $\vec{n}$ is the vector normal to the surface which by definition is

$$\sin\theta\vec{n} = \vec{t}_1 \times \vec{t}_2 \qquad (B15)$$

or

$$\vec{n} = \frac{1}{h_1 h_2 \sin\theta}\left[-b\left(\frac{\partial\bar{z}}{\partial\phi}\right)i - \left(\frac{\partial\bar{x}}{\partial\phi}\frac{\partial\bar{z}}{\partial y} - \frac{\partial\bar{x}}{\partial y}\frac{\partial\bar{z}}{\partial\phi}\right)j + b\left(\frac{\partial\bar{x}}{\partial\phi}\right)k\right] \qquad (B16)$$

With the use of (B9), the expression (B13) can be written as

$$\vec{K} = \frac{1}{h^2}\frac{d^2\vec{r}}{dP^2} - \frac{1}{h^3}\frac{d\vec{r}}{dP}\frac{dh}{dP} = \frac{1}{h^2}\left(\frac{d^2\bar{x}}{dP^2}i + \frac{d^2\bar{y}}{dP^2}j + \frac{d^2\bar{z}}{dP^2}k\right)$$

$$- \frac{1}{h^4}\left(\frac{d\bar{x}}{dP}i + \frac{d\bar{y}}{dP}j + \frac{d\bar{z}}{dP}k\right)\left(\frac{d^2\bar{x}}{dP^2}\frac{d\bar{x}}{dP} + \frac{d^2\bar{y}}{dP^2}\frac{d\bar{y}}{dP} + \frac{d^2\bar{z}}{dP^2}\frac{d\bar{z}}{dP}\right) \qquad (B17)$$

The geodesic curvature K_{g1} for curve y = const. is

$$K_{g1} = -(\vec{t}_1 \times \vec{n}) \cdot \vec{K}_1 \qquad (B18)$$

The minus sign on the right-hand side of (B18) is introduced to obtain $K_{g1} = -(1/h_1 h_2)(\partial h_1/\partial y)$ in the case of orthogonal coordinate system. With ϕ as the parameter, the expression for $\vec{K}_1$ is

74

$$\vec{K}_1 = \frac{1}{h_1^2}\left[\frac{\partial^2 \bar{x}}{\partial \phi^2}\,\vec{i} + \frac{\partial^2 \bar{z}}{\partial \phi^2}\,\vec{k}\right] - \frac{1}{h_1^4}\left[\left(\frac{\partial \bar{x}}{\partial \phi}\,\vec{i} + \frac{\partial \bar{z}}{\partial \phi}\,\vec{k}\right)\left(\frac{\partial^2 \bar{x}}{\partial \phi^2}\frac{\partial \bar{x}}{\partial \phi} + \frac{\partial^2 \bar{z}}{\partial \phi^2}\frac{\partial \bar{z}}{\partial \phi}\right)\right] \qquad \text{(B19)}$$

Introducing the expressions (B10), (B16) and (B19) into (B18) gives, after simplifications

$$K_{g_1} = \frac{-1}{h_1^4 h_2 \sin\theta}\left(\frac{\partial \bar{x}}{\partial \phi}\frac{\partial \bar{z}}{\partial y} - \frac{\partial \bar{x}}{\partial y}\frac{\partial \bar{z}}{\partial \phi}\right)\left(\frac{\partial^2 \bar{x}}{\partial \phi^2}\frac{\partial \bar{z}}{\partial \phi} - \frac{\partial^2 \bar{z}}{\partial \phi^2}\frac{\partial \bar{x}}{\partial \phi}\right) \qquad \text{(B20)}$$

The geodesic curvature for a curve ϕ = const. is given by

$$K_{g_2} = (\vec{t}_2 \times \vec{n}) \cdot \vec{K}_2 \qquad \text{(B21)}$$

With y as the parameter, the expression for $\vec{K}_2$ is

$$\vec{K}_2 = \frac{1}{h_2^2}\left[\frac{\partial^2 \bar{x}}{\partial y^2}\,\vec{i} + \frac{\partial^2 \bar{z}}{\partial y^2}\,\vec{k}\right] - \frac{1}{h_2^4}\left[\frac{\partial \bar{x}}{\partial y}\,\vec{i} + b\vec{j} + \frac{\partial \bar{z}}{\partial y}\,\vec{k}\right]\left[\frac{\partial^2 \bar{x}}{\partial y^2}\frac{\partial \bar{x}}{\partial y} + \frac{\partial^2 \bar{z}}{\partial y^2}\frac{\partial \bar{z}}{\partial y}\right] \qquad \text{(B22)}$$

The expression for the geodesic curvature K_{g_2} is obtained by substitution of (B11), (B16) and (B22) into (B21):

$$K_{g_2} = \frac{1}{h_1 h_2^4 \sin\theta}\left[\left(\frac{\partial \bar{x}}{\partial \phi}\frac{\partial \bar{z}}{\partial y} - \frac{\partial \bar{x}}{\partial y}\frac{\partial \bar{z}}{\partial \phi}\right)\left(\frac{\partial^2 \bar{x}}{\partial y^2}\frac{\partial \bar{z}}{\partial y} - \frac{\partial^2 \bar{z}}{\partial y^2}\frac{\partial \bar{x}}{\partial y}\right) + b^2\left(\frac{\partial^2 \bar{x}}{\partial y^2}\frac{\partial \bar{x}}{\partial \phi} + \frac{\partial^2 \bar{z}}{\partial y^2}\frac{\partial \bar{z}}{\partial \phi}\right)\right]$$

$$\text{(B23)}$$

As discussed in the beginning of this section, the program reads in n pairs (n can be variable along span) of $\bar{x}_i$, $\bar{z}_i$ values at each spanwise station $\bar{y}_j$. Then the use of equations (B1) and (B5) gives the corresponding ϕ_i. Since the desired chordwise outputs are read in as $(\xi/c)_p$, we again use equation (B5) to obtain ϕ_p. Next, the tables of $\bar{x}_i$ and $\bar{z}_i$ vs ϕ_i at each $\bar{y}_j$ are fitted with cubic splines to obtain interpolated values of $\bar{x}_p$, $\bar{z}_p$, and $\partial \bar{z}_p/\partial \phi$ corresponding to ϕ_p. Here the cubic splines are not used to obtain the second derivatives because of inherent inaccuracies. Instead, we use a Fourier fit with sigma-smoothing. The end result is smoothed $\partial \bar{z}_p/\partial \phi$ values and $\partial^2 \bar{z}_p/\partial \phi^2$. Because of relationships (B1) and (B5), the derivatives of $\bar{x}$ can be calculated as follows:

75

$$\frac{\partial \bar{x}_p}{\partial \phi} = \tan\alpha \ \frac{\partial \bar{z}_p}{\partial \phi} + \frac{c \ \sin\phi_p}{\cos\alpha} \qquad (B24)$$

$$\frac{\partial^2 \bar{x}_p}{\partial \phi^2} = \tan\alpha \ \frac{\partial^2 \bar{z}_p}{\partial \phi^2} + \frac{c \ \cos\phi_p}{\cos\alpha} \qquad (B25)$$

To obtain the derivatives with respect to y at desired output locations $\bar{y}_s$, we spline-fit the $\bar{x}_p$ and $\bar{z}_p$ values at constant ϕ_p vs y_j. The first derivatives are again not used directly, instead they are put through the Fourier smoothing procedure and simultaneously interpolated for values at $\bar{y}_s$ together with the second derivatives. To obtain the $\bar{x}_p$ and $\bar{z}_p$ values and their derivatives with respect to ϕ at $\bar{y}_s$ cubic spanwise interpolation is used.

After the derivatives are determined the quantities h_1, h_2, ϕ, K_{g_1} and K_{g_2} are calculated from the relationships given previously. To calculate the remaining quantities K_{12} and K_{21} requires extra care at the leading edge because the terms K_1 and $1/h_1 \ \partial\theta/\partial\phi$ are large and of opposite sign. In effect, the sum of these two terms is similar to a third-order derivative. The best results were obtained by sigma-smoothing the calculated K_1 and K_2 values and applying the same technique to the calculation of θ-derivatives. It is also helpful to extend the wing definition input data a long way around the leading edge on the opposite surface if boundary-layer calculations involve the leading edge.

REFERENCES

1. Hunt, J. L., Bushnell, D. M., and Beckwith, I. E.: Finite-Difference Analysis of the Compressible Turbulent Boundary Layer on a Blunt Swept Slab with Leading-Edge Blowing. Analytical Methods in Aircraft Aerodynamics, Paper 19, NASA SP-228, Symposium held at NASA Ames Research Center, Moffett Field, Calif., Oct. 1969, pp. 417-472; see also TN D-6203, March 1971, NASA.

2. Bushnell, D. M. and Beckwith, I. E.: Calculation of Nonequilibrium Hypersonic Turbulent Boundary Layers and Comparisons with Experimental Data. AIAA Journal, Vol. 8, p. 1462, 1970.

3. Adams, J. C.: Three-Dimensional Compressible Turbulent Boundary Layer on a Sharp Cone at Incidence in Supersonic Flow. International Journal of Heat and Mass Transfer, Vol. 17, June 1974, pp. 581-593.

4. Bradshaw, P.: Calculation of Three-Dimensional Turbulent Boundary Layers. Journal of Fluid Mechanics, Vol. 46, Pt. 3, April 1971, pp. 417-445.

5. Nash, J. F.: The Calculation of Three-Dimensional Turbulent Boundary Layers in Incompressible Flow. Journal of Fluid Mechanics, Vol. 37, July 1969, pp. 625-642.

6. Nash, J. F. and Scruggs, R. M.: Three-Dimensional Compressible Boundary-Layer Computations for a Finite Swept Wing. NASA CR-112158, 1972.

7. Harris, J. E. and Morris, D. J.: Solution of the Three-Dimensional Compressible Laminar and Turbulent Boundary-Layer Equations with Comparisons to Experimental Data. Presented at the 4th International Conference on Numerical Methods in Fluid Dynamics, Boulder, Colo., June 1974.

8. Kendall, R. M., Bonnett, W. S., Nardo, C. T. and Abbett, M. J.: Three-Dimensional Compressible Boundary Layers of Reacting Gases Over Realistic Configurations. Aerodynamic Analysis Requiring Advanced Computers, Pt. I, NASA SP-347, pp. 77-99.

9. Wortman, A.: Three-Dimensional Turbulent Boundary-Layer Calculations — Exact and Simplified Solution. AIAA 8th Fluid and Plasma Dynamics Conference, Hartford, Connecticut, June 16-18, 1975; AIAA Paper No. 75-854.

10. Cebeci, T.: Calculation of Three-Dimensional Boundary Layers. I. Swept Infinite Cylinders and Small Cross Flow. AIAA Journal, Vol. 12, June 1974, pp. 779-786.

11. Keller, H. B. and Cebeci, T.: Accurate Numerical Methods for Boundary Layers. II. Two-Dimensional Turbulent Flows. AIAA Journal, Vol. 10, Sept. 1972, pp. 1197-1200.

12. Cebeci, T.: Calculation of Three-Dimensional Boundary Layers. II. Three Dimensional Flows in Cartesian Coordinates. AIAA Journal, Vol. 13, No. 8, Aug. 1975, pp. 1056-1064.

13. Cebeci, T., Kaups, K. and Moser, A.: Calculation of Three-Dimensional Boundary Layers. III. Three-Dimensional Flows in Curvilinear Orthogonal Coordinates. AIAA Journal, Vol. 14, No. 8, Aug. 1976, pp. 1090-1094.

14. Cebeci, T. and Smith, A.M.O.: Analysis of Turbulent Boundary Layers. Academic Press, New York, 1974.

15. Squire, L. C.: The Three-Dimensional Boundary-Layer Equations and Some Power Series Solutions. R&M No. 3006, 1957.

16. Hansen, A. G.: Compressible, Three-Dimensional Laminar Boundary Layers — A Survey of Current Methods of Analysis. Douglas Paper No. 3105, Sept. 1964.

17. Isaacson, E. and Keller, H. B.: Analysis of Numerical Methods. Wiley, New York, 1966.

18. Keller, H. B.: A New Difference Scheme for Parabolic Problems. Numerical Solutions of Partial Differential Equations, II. J. Bramble (ed.) Academic Press, New York, 1970.

19. Brebner, G. G. and Wyatt, L. A.: Boundary-Layer Measurements at Low Speeds on Two Wings of 45° and 55° Sweep. Aeronautical Research Council Current Papers, C.P. No. 554, 1961.

78

20. Hess, J. L.: The Problem of Three-Dimensional Lifting Potential Flow and Its Solution by Means of Surface Singularity Distribution. Computer Methods in Applied Mechanics and Engineering, Vol. 4, No. 3, Nov. 1974.

21. Harris, C. D.: Wind-Tunnel Measurements of Aerodynamic Load Distribution on a NASA Supercritical-Wing Research Airplane Configuration. NASA TMX-2469, 1972.